

Cyclic activity of Fuego de Colima volcano (Mexico): insights from satellite thermal data and non-linear models

Silvia Massaro^{1*}, Antonio Costa², Roberto Sulpizio^{1,3}, Diego Coppola⁴, Lucia Capra⁵

¹Istituto per la Dinamica dei Processi Ambientali – Consiglio Nazionale delle Ricerche, Via R. Cozzi 53, 20125, Milan (Italy)

²Istituto Nazionale di Geofisica e Vulcanologia, Via D. Creti 12, 40128, Bologna (Italy)

³Dipartimento di Scienze della Terra e Geoambientali, Università di Bari, Via Orabona 4, 70125, Bari (Italy)

⁴Dipartimento di Scienze della Terra, Università di Torino, Via Valperga Caluso, 35, 10129, Turin (Italy)

⁵Centro de Geociencias UNAM, Campus Juriquilla, Queretaro (Mexico)

*Corresponding Author: Silvia Massaro (silvia-massaro@libero.it)

Abstract

The Fuego de Colima volcano (Mexico) showed a complex eruptive behaviour with periods of rapid and slow lava dome growth, punctuated by explosive activity. We reconstructed the weekly discharge rate average between 1998 and 2018 by means of satellite thermal data integrated with published discharge rate data. By using spectral and wavelet analysis, we found a multi-year long-, multi-month intermediate-, and multi-week short-term cyclic behaviour during the period of the investigated eruptive activity, as those of many others dome-forming volcanoes. We use numerical modelling in order to investigate the non-linear cyclic eruptive behaviour considering a magma feeding system composed of a dual or a single magma chamber connected to the surface through an elastic dyke [developing](#) into a cylinder conduit in the shallowest part. We investigated the cases in which the periodicity is controlled by i) the coupled deep-shallow magma reservoirs, ii) the single shallow chamber, and iii) the elastic shallow dyke when is fed by a fixed influx rate or a constant pressure. [Due to the limitations of the current modelling approach, there is no a single configuration that can reproduce all the periodicities on the three different time scales.](#) The model outputs indicate that the observed multi-year periodicity (1.5-2.5 years) can be described by the fluctuations controlled by a shallow magma chamber with a volume of 20-50 km³ coupled with a deep reservoir of [ca.](#) 500 km³, connected through a deep elastic dyke. The multi-month periodicity (ca. 5 - 10 months) appears to be controlled by the shallow magma chamber for the same range of volumes. The short-term multi-week periodicity (ca. 2.5 - 5 weeks) can be reproduced considering a fixed influx rate or constant pressure at the base of the shallower dyke. This work provides new insights on the non-linear cyclic behaviour of Fuego de Colima, and a general framework for the comprehension of eruptive behaviour of andesitic volcanoes.

37 1. Introduction

38 Lava dome forming eruptions are relatively long-lived events, lasting from several months to
39 several decades (e.g. Merapi, Indonesia, Siswamidjoyo et al., 1995; Kelut, Indonesia, De B elizal et
40 al., 2012; Fuego de Colima, Mexico, Lamb et al., 2014; Santiaguito, Guatemala, Harris et al.,
41 2002), and usually punctuated by dome collapses and explosive (Vulcanian) episodes. Discharge
42 rates can change widely over a range of time scales, reflecting the physical mechanisms involved in
43 the transfer of magma to the Earth’s surface (Melnik et al., 2008; Odbert and Wadge 2009). Dome
44 growth shows a periodic behaviour, which has been commonly observed at several volcanoes,
45 including Santiaguito (Guatemala, Harris et al., 2003), Mt St Helens (USA, Swanson and Holcomb,
46 1990), and Soufriere Hills (Montserrat, Voight et al., 1998; Loughlin et al., 2010; Wadge et al.,
47 2010; Nicholson et al., 2011). Periodic behaviours can be complex, showing systematic or non-
48 systematic temporal changes as the eruption progresses (Denlinger and Hoblitt, 1999; Costa et al.,
49 2007a; Melnik et al., 2008; Bernstein et al., 2013; Wolpert et al., 2016), and may be characterized
50 by short-, intermediate- and long-term periodicities (Costa et al., 2007a; Melnik et al., 2008; Costa
51 et al., 2012; 2013; Melnik and Costa, 2014). Short- and intermediate-term periodicities (hours or
52 weeks) are generally explained by the upper conduit pressurization related to the non-linear ascent
53 of magma flow (Denlinger and Hoblitt, 1999; Melnik and Sparks, 1999; Voight et al., 1999; Wylie
54 et al., 1999; Ozerov et al., 2003; Lensky et al., 2004, Costa et al., 2007a,b; 2012; Kozono and
55 Koyaguchi, 2009; 2012). This is because the lower part of the dyke-conduit can act as a capacitor
56 that allows magma to be stored temporarily and released during the more intense phase of discharge
57 (Costa et al., 2007a,b; Melnik et al., 2008; Costa et al. 2012; 2013). The long-term periodicity, with
58 time scales from several months to decades (Voight et al., 2000; Belousov et al., 2002; Sparks and
59 Young, 2002; Wadge et al., 2006), is usually controlled by pressure variations in magma reservoirs
60 (Barmin et al., 2002; Costa et al., 2007b; Melnik et al., 2008; Melnik and Costa, 2014). Since
61 historical times, the Fuego de Colima volcano (Mexico; Fig.1a) has been characterised by decade-
62 lasting cycles of dome growth alternating with Vulcanian explosions, ended with sub-Plinian

63 | eruptions (the last two occurred in 1818 and 1913; Luhr, 2002; Saucedo et al., 2005; Norini et al.,
64 | 2010; Heap et al., 2014; Massaro et al., 2018a). The most recent cycle started after the 1913
65 | eruption, and it is characterized by lava domes extruded with minor seismicity at high magma
66 | temperatures (960-1020°C; Savov et al., 2008). As for other dome eruptions (Sparks, 1997), dome
67 | growth at Fuego de Colima can be explained by complex non-linear pressure variations during
68 | magma ascent from magma reservoirs (e.g. Melnik and Costa, 2014), cooling, crystallization,
69 | degassing (e.g. Melnik and Sparks, 1999; Lensky et al., 2004; Nakanishi and Koyaguchi, 2008;
70 | Kozono and Koyaguchi, 2012) and upper conduit geometric configurations characterized by
71 | multiple pathways (e.g. Lavallée et al., 2012; Reubi et al., 2015).

72 | Two magma chambers located at different depths characterize the feeding system of Fuego de
73 | Colima volcano (Fig. 1b), with roofs located at ca. 6 (shallow magma chamber) and ca. 15 km
74 | (deep magma chamber) of depth, as indicated by petrographic studies (Macias et al., 2017) and
75 | geophysical data (Spica et al., 2017).

76 | The purpose of this study is to investigate the existence of pattern of fluctuations in discharge rates
77 | during the 1998-2018 erupted activity at Fuego de Colima volcano. The available geological,
78 | geophysical, and petrological data for this recent activity provide a remarkable opportunity to
79 | improve the characterization and our understanding about the physical processes underlying cyclic
80 | extrusion of lava domes. In particular, we used thermal remote sensing data along with published
81 | effusion rates for reconstructing the oscillatory magma discharge rate behaviour of effusive activity
82 | at Colima.

83 | The availability of satellite thermal images in the last decade has strengthened the use of thermal
84 | data for observing volcanic activity (e.g. Ramsey and Harris, 2012), especially in studying the
85 | relationships with lava discharge rates (Coppola et al., 2009; Harris et al., 2010; Garel et al., 2012).
86 | Coppola et al. (2013) propose that the radiant density of effusive/extrusive activity can be used to
87 | estimate lava discharge rates and erupted volumes by means of empirical relationship based on SiO₂
88 | content of the erupted lava. Although it is still under debate, the so-called “thermal approach”

89 (Dragoni and Tallarico, 2009) offers a good way for monitoring volcanic activity, especially when
90 direct observations are limited or absent. Here we focus our attention to the dynamics of
91 fluctuations in magma discharge rate at different timescales at Fuego de Colima volcano during
92 1998-2018. By using time series analytical techniques (i.e. Fourier and wavelet analysis) we have
93 identified three fundamental periodicities in subsets of the time series: i) long-term (ca. 1.5-2.5
94 years), ii) intermediate-term (ca. 5-10 months), iii) short-term (ca. 2.5-5 weeks), similar to those
95 observed at many lava-dome eruptions (e.g. Costa et al., 2012; Melnik and Costa, 2014; Christopher
96 et al., 2015). These periodicities were compared with numerical simulations provided by the model
97 of Melnik and Sparks (2005) as generalized by Costa et al. (2007a) for accounting the presence of a
98 shallow dyke, and Melnik and Costa (2014) for describing the control of a coupled dual chamber
99 system. Numerical modelling of the different parts of the pumbling system can successfully
100 reproduce the first-order cyclic behaviour of Fuego de Colima during the 1998-2018 erupted
101 activity. Our results highlighted that the dual magma chamber dynamics controls the long-term
102 periodicity evident during 2002-2006 and 2013-2016, while the single magma chamber dynamics
103 are more effective to explain the intermediate-term periodicity in the same periods. Finally, the
104 shallow dyke dynamics regulate the multi-week cycles observed during 2002-2006 and 2011-2016.
105 The present work is divided in five main sections. The first describes the historical activity of the
106 Fuego de Colima, with particular attention to the recent period, from 1998 to 2018. The second
107 section describes the methods applied to the dataset composed of the satellite thermal data
108 integrated with published data. The third section is dedicated to the input and target data used for
109 numerical simulations. The fourth section presents the results obtained by the spectral and wavelet
110 analyses. This latter allows us to establish significance levels for the wavelet power spectrum. The
111 periodicities observed in this spectrum were compared to the results obtained by numerical
112 simulations. The last fifth section contains a discussion on the eruptive behaviour occurred at Fuego
113 de Colima during 1998-2018, providing new insights from the observed data and non-linear models.

114

115 2. The historical activity of Fuego de Colima volcano

116

117 Since historical times Fuego de Colima represents the most active volcano in Mexico, posing a
118 serious threat to all surrounding populations (Cortés et al., 2005; Gavilanes-Ruiz et al., 2009;
119 Bonasia et al., 2011; [Roverato et al., 2011](#)). The earliest accounts of the volcano activity can be
120 found in *Historia Antigua de Mexico* (Clavijero, 1780), where the destructive effects of its
121 explosive activity are carefully described (Bretón-Gonzales et al., 2002). The historical activity of
122 Fuego de Colima was described and interpreted by several authors (Luhr and Carmichael, 1980;
123 Medina-Martínez, 1983; De la Cruz-Reyna, 1993; Bretón-Gonzales et al., 2002; Luhr, 2002). The
124 Fuego de Colima has shown a transitional eruptive behaviour spanning from effusive to explosive
125 activity, dominated by dome growth and Vulcanian eruptions. Occasionally sub-Plinian events
126 occurred (1576, 1606, 1690, 1818 and 1913), indicating a recurrence time of approximately 100
127 years (De la Cruz-Reyna, 1993; Luhr, 2002; Saucedo et al., 2005; Gavilanes-Ruiz et al., 2009;
128 Massaro et al. 2018a). The sub-Plinian event occurred in 1913 (Saucedo et al., 2010) is the largest
129 historical eruption and it has been used as benchmark for volcanic hazard studies (Martin Del Pozzo
130 et al., 1995; Saucedo et al., 2005; Bonasia et al., 2011).

131

132 2.1. The 1998-2018 eruptive activity

133 The 1998-2018 is the only period of post 1913 activity for which there is sufficiently available
134 information to explore the cyclic activity of Fuego de Colima. Different periods of effusion (domes
135 and lava flows) punctuated by Vulcanian eruptions and dome collapses characterised the volcano
136 activity between 1998 and 2018 (Savov et al., 2008; Varley et al., 2010a; Hutchinson et al., 2013;
137 Mueller et al., 2013; Zobin et al., 2015; GVP, 2017). The duration of extrusive activity and magma
138 discharge rate varied through time, that was generally divided into five eruptive phases up to 2015;
139 I) 1998-1999; II) 2001-2003; III) 2004-2005; IV) 2007-2011; V) 2013-2015 (Zobin et al., 2015;
140 Aràmbula-Mendoza et al., 2018).

141 The first dome extrusion started in November 1998, and quickly filled the 1994 explosion crater,
142 forming lava flows that descended the southern flanks of the Fuego de Colima cone during most of
143 1999 ($> 5 \text{ m}^3 \text{ s}^{-1}$ in average for Mueller et al., 2013; $4.11 \text{ m}^3 \text{ s}^{-1}$ in average for Reubi et al., 2013).
144 At the beginning, this dome grew rapidly (ca. $4.4 \text{ m}^3 \text{ s}^{-1}$) reaching a volume of ca. $3.8 \times 10^5 \text{ m}^3$ in
145 24 hours. During this period the effusion rate reached a peak value around $30 \text{ m}^3 \text{ s}^{-1}$ (Navarro-
146 Ochoa et al., 2002; Zobin et al., 2005; Reubi et al., 2015) and showed a cyclic damped behaviour
147 soon after. During 1999-2001 a series of explosions destroyed the dome and excavated a large
148 apical crater (Bretòn-Gonzales et al., 2002).

149 A slow outpouring of lava ($< 1 \text{ m}^3 \text{ s}^{-1}$ for Mueller et al., 2013; $0.17 \text{ m}^3 \text{ s}^{-1}$ for Reubi et al., 2013;
150 2015) resumed in May 2001 and continued for 22 months. In February 2002, the lava dome
151 overflowed the crater rims producing lava flows. During this eruptive phase, the magma extruded
152 from three separate vents with only minor explosive activity, at a rate of ca. $0.9 \text{ m}^3 \text{ s}^{-1}$ (GVP, 2002).
153 Vulcanian explosions dismantled the dome during July and August 2003 (GVP, 2003).

154 In September 2004, low-frequency seismic swarms heralded the onset of the new effusive phase
155 (Varley et al., 2010a; Arámbula-Mendoza et al., 2011; Lavallée et al., 2012) with a small increase
156 in average discharge rate of $0.6 \text{ m}^3 \text{ s}^{-1}$ (Reubi et al., 2013; 2015). The lava dome building occurred
157 from the end of September until the beginning of November, with a magma effusion rate up to 7.5
158 $\text{m}^3 \text{ s}^{-1}$ in October (Zobin et al., 2008; 2015). The effusive activity was accompanied and followed
159 by intermittent Vulcanian explosions. The explosive activity diminished in intensity during
160 December 2004-January 2005. From February to September 2005, effusion and large explosions
161 occurred.

162 In the following months, small, short-lived domes were observed, with an estimated effusion rate
163 between $1.2 - 4.6 \text{ m}^3 \text{ s}^{-1}$ (Varley et al., 2010b; Reubi et al., 2015). In May and June, the explosive
164 activity produced pyroclastic density currents reaching distances up to 5.4 km from the volcano
165 summit (Varley et al., 2010a). In February 2007, a new lava dome began to grow and explosions
166 were reported in the period between January 2009 and March 2011. The 2007-2011 period of dome

167 extrusion represents the slowest growth rate in the recent history of Fuego de Colima. Hutchinson et
168 al. (2013) calculated a mean effusion rate of ca. $0.02 \text{ m}^3 \text{ s}^{-1}$ from 2007 to 2010 using digital
169 photographic data, in good accordance with Zobin et al. (2015) that reported extrusion rates of 0.03
170 $\text{m}^3 \text{ s}^{-1}$ during 2007. Mueller et al. (2013) estimated the magma extrusion rate between 0.008 ± 0.003
171 $\text{m}^3 \text{ s}^{-1}$ to $0.02 \pm 0.007 \text{ m}^3 \text{ s}^{-1}$ during 2010, which dropped down to $0.008 \pm 0.003 \text{ m}^3 \text{ s}^{-1}$ again in
172 March 2011. On 21 June 2011 an explosion heralded the cessation of dome growth and marked the
173 end of the effusive period.

174 After 1.5 years of rest, in January 2013 a sequence of explosions cored out the 2011 dome and
175 generated pyroclastic density currents that reached distances of up to 2.8 km from the summit
176 (GVP, 2013). From March to October, the calculated discharge rate was in the range of $0.1 - 0.2 \text{ m}^3$
177 s^{-1} (Reyes-Dávila et al., 2016). Successively, the mid-low explosive activity took place up to
178 February-March 2014, until a new pulse of magma observed in July, with an approximate rate of 1-
179 $2 \text{ m}^3 \text{ s}^{-1}$ (Aràmbula-Mendoza et al., 2018). On 11 January 2015, a new lava dome was observed
180 inside the crater (Thiele et al., 2013) and its growth continued until July, with effusion rate of ca.
181 $0.27 \text{ m}^3 \text{ s}^{-1}$ (Zobin et al., 2015). Between 10-11 July 2015 the recent dome was destroyed by the
182 most intense activity since the 1913 eruption (Capra et al., 2016; Reyes-Dávila et al., 2016). In the
183 2013-2015 period, the average extrusion rate was of ca. $0.2 \text{ m}^3 \text{ s}^{-1}$ (Thiele et al., 2017), with peak
184 values $> 10 \text{ m}^3 \text{ s}^{-1}$ (Varley, 2015). After that, the eruptive activity ceased until January 2016 when
185 daily ash plumes started to occur along with active lava flows and explosions. In early July a new
186 dome began to grow, overtopping the crater rim. A large explosion was recorded on 10 July 2016,
187 followed by daily and multiple-daily ash plumes up to the end of year. Multiple flows descended
188 from lava dome during September-December. In 2017 frequent strong explosions and ash emissions
189 were recorded until March. Through June decreasing seismicity and minor landslides were reported
190 with no evidence of effusive activity or new dome growth (GVP, 2017). Here we provide a more
191 systematic overview of the 1998-2018 erupted activity, obtained by satellite thermal data along with
192 some published data, explained in the following section.

193 3. Methods

194 We analysed the thermal energy spectrum of Fuego de Colima volcano available from March 2000
195 to October 2018, detected Middle Infrared Observation of Volcanic activity (MIROVA) hot-spot
196 detection system (Coppola et al., 2016). The period 1998-1999 was integrated using published
197 discharge rates (Navarro-Ochoa et al., 2002; Zobin et al., 2005). The MIROVA NRT system is
198 based on the near real time (NRT) analysis of the MODerate resolution Imaging Spectroradiometer
199 (MODIS) data, distributed by the LANCE-MODIS data system (<http://modis.gsfc.nasa.gov/>).

200 The thermal emission from an object is attenuated by the atmosphere resulting from absorption by
201 gases and scattering by particles. MIROVA system focuses on the Middle InfraRed region (MIR),
202 which shows the lowest attenuation levels, to better detect and analyse thermal radiation emitted
203 from volcanic sources. While the standard MODIS forward processing delivers Aqua and Terra
204 images within 7-8 hours of real time, LANCE-MODIS allows for the creation of MIROVA radiant
205 flux timeseries within 1-4 hours from the satellite overpass (www.mirovaweb.it). This thermal data
206 collection was converted into lava discharge rate estimates and integrated with some published data
207 in order to reconstruct the weekly mean discharge rate spectrum from 1998 to 2018 (Fig. 2a).

208 In this work, we refer to Coppola et al. (2013), who describes the relationship between the heat lost
209 by lava thermal radiance variations and discharge rates, by means of a unique, empirical parameter.
210 They compared the energy radiated during several distinct eruptions to the erupted lava volumes
211 (m^3). The relationship between the Volcanic Radiated Energy (*VRE*) and the erupted volume was
212 defined by introducing the concept of radiant density (c_{rad} , in J m^{-3}). This parameter is analysed as a
213 function of the SiO_2 content and the bulk rheological properties of the related lava bodies. It is
214 strongly controlled by the characteristic thickness of the active lavas at the time of a satellite
215 overpass, whereas the effects of variable degree of insulation, morphology and topographic
216 conditions produce only a limited range of variability ($\pm 50\%$) (Coppola et al., 2013). For the Fuego
217 de Colima we used a value of $c_{rad} = 3.90 \times 10^7 \text{ (J m}^{-3}\text{)}$ for a SiO_2 content of 59.6% (Savov et al.,

218 2008; Coppola et al., 2013). We obtained the cumulative volumes of effusion per year (from 2000
219 to 2018) considering the ratio between the average *VRE* estimations and c_{rad} . It is important to stress
220 that the instrumental limit of the MIROVA system is not able to detect thermal anomalies below
221 0.5–1 MW. Since we used a radiant density (c_{rad}) of $3.90 \times 10^7 \text{ J m}^{-3}$, the minimum reliable value of
222 discharge rate is $0.01 \text{ m}^3 \text{ s}^{-1}$ (Coppola et al., 2013). As reported by Coppola et al. (2016), the
223 thermal data obtained from MIROVA are not correct due to the presence/attenuation of clouds. For
224 this reason, the estimates of effusion rates and volumes are to be considered as minimum estimates.

225 Because the 2002-2006 and 2013-2016 intervals are the most active in the analysed period, we
226 firstly applied the Fourier analysis to the monthly average of discharge rates (Fig. 2b) of these time
227 intervals, in order to explore the modal spectrum of the signal. Although Fourier analysis is well
228 suited to the quantification of constant periodic components in a time series, it cannot recognise
229 signals with time-variant frequency content. Whereas a Fourier Transform analysis may determine
230 all the spectral components embedded in a signal, it does not provide any information about timing
231 of occurrence. To overcome this problem, several solutions have been developed in the past
232 decades that are able to represent a signal in the time and frequency domain at the same time.

233 The aim of these approaches is to expand a signal into different waveforms with local time–
234 frequency properties well adapted to the signal structure (Cazellas et al., 2008). In order to get
235 information on the amplitude of the periodic signals within the Fuego de Colima (MIROVA) time
236 series, we performed a wavelet analysis by decomposing the weekly time series (Fig. 2a) into
237 time/frequency space (Fig. 3).

238 Wavelet analysis is a powerful tool largely used in many scientific fields (i.e., ecology, biology,
239 climatology, geophysics) and engineering. It is especially relevant to the analysis of non-stationary
240 systems (i.e., systems with short-lived transient components, Cazellas et al., 2008). [The wavelet
241 analysis is well suited for investigations of the temporal evolution of aperiodic and transient signals
242 \(Lau and Weng, 1995; Mallat, 1998\).](#)

243 For this study, practical details in applying wavelet analysis were taken from Torrence and Compo
 244 (1998) and Odbert and Wadge (2009). It is worth noting that wavelet analysis considers a wave
 245 that decays over a finite time and whose integral over infinite time is zero. Many forms of wavelet
 246 (called “wavelet functions” $\psi(\eta)$, or “mother functions”, which depend on a non-dimensional time
 247 parameter “ η ”) have been designed for analytical use (Farge, 1992; Weng and Lau, 1994;
 248 Daubechies, 1994), each with its own characteristics that make it suitable for certain applications.
 249 The choice of the wavelet can influence the time and the scale resolution of the signal
 250 decomposition. Wavelet analysis is popular in geosciences (Trauth, 2006), as it does not require
 251 any a priori understanding of the system generating the time series.

252 Our time series (weakly average discharge rates acquired mainly by the MIROVA system; Fig. 2a),
 253 called (x_n) , has equal time spacing ($\delta t = 7$ days) and number of points $n = 0 \dots N-1$. Using the
 254 approximately orthogonal Morlet function as wavelet function $\psi(\eta)$ (it must have zero mean and
 255 be localized in both time and frequency space; Farge, 1992), we here define the wavelet transform
 256 $W_n(s)$ as the convolution of x_n with a scale (s) and translated version of $\psi_0(\eta)$ (mother function). In
 257 formula:

$$258 \quad W_n(s) = \sum_{n'=0}^{N-1} x_{n'} \psi * \left[\frac{(n' - n)\delta t}{s} \right] \quad (1)$$

259 where the (*) indicates the complex conjugate. The scale s should be equal to approximately $2\delta t$,
 260 according to the Nyquist theorem. Therefore, the smallest wavelet we could possibly resolve is $2\delta t$,
 261 thus we choose $s_0 = 14$ days. Generally, $\psi(\eta)$ is a complex function, therefore the wavelet transform
 262 is also complex. It is possible to reconstruct the “local” wavelet power spectrum as the absolute-
 263 value squared of the wavelet coefficients, $|W_n(s)|^2$. The way to compute the wavelet transform for a
 264 time series is to find the Fourier transform of both the wavelet function (Morlet in our case) and the
 265 time series. Following Torrence and Compo (1998), we made the normalization by dividing by the
 266 square-root of the total wavelet variance (σ^2).

267 Usually, a periodic component in a time series may be identified in a power spectrum if it has
268 distinctly greater power than a mean background level (that would correspond to a Gaussian
269 background noise) (Odbert and Wadge, 2009). However, the spectra generated from many
270 geophysical systems indicate that the noise in time series data tends not to have a Gaussian
271 distribution (Vila et al., 2006) but it can be better described by coloured noise, specifically red noise
272 (Fougere, 1985). For this reason we use a simple model for red noise given by the univariate lag-1
273 autoregressive or Markov process (Torrence and Compo, 1998) in order to determine the
274 significance levels for our wavelet spectrum. These background spectra are used to establish a null
275 hypothesis for the significance of a peak in the wavelet power spectrum. The null hypothesis is
276 defined for the wavelet power spectrum considering that the time series has a mean power
277 spectrum: if a peak in the wavelet power spectrum is significantly above this background spectrum,
278 then it can be assumed to be a true feature with a certain percentage of confidence. For definitions,
279 “significant at the 5% level” is equivalent to “the 95% confidence level” (Torrence and Compo,
280 1998). The confidence interval is defined as the probability that the true wavelet power at a certain
281 time and scale lies within a certain interval about the estimated wavelet power (Torrence and
282 Compo, 1998). Because we deal with finite-length time series, errors occur at the beginning and end
283 of the wavelet power spectrum. A solution is to pad the end of the time series with zeroes to bring
284 the total length N up to the next-higher power of two, thus limiting the edge effects. However,
285 padding with zeroes introduces discontinuities at the endpoints and, especially towards larger
286 scales, decreasing the amplitude near the edges as more zeroes enter the analysis (Torrence and
287 Compo, 1998). The cone of influence (COI) is the region of the wavelet spectrum **beyond** which
288 edge effects become important. The criterion for applying wavelet analysis is very similar to those
289 employed with classic spectral methods. In other words, the wavelet transform can be regarded as a
290 generalization of the Fourier transform, and by analogy with spectral approaches, we compute the
291 local wavelet power spectrum as described above. Successively, this can be compared with the
292 “global” wavelet power spectrum which is defined as the averaged variance contained in all wavelet

293 coefficients of the same frequency (Torrence and Compo, 1998; Cazellas et al., 2008).

294 Numerical simulations have been carried out using the magma flow model of Melnik and Costa
295 (2014), who generalized the model proposed by Melnik and Sparks (2005) [and Costa et al. \(2007a\)](#)
296 for a magma chamber connected to a dyke that [develops](#) into a cylindrical conduit near surface. In
297 particular, the model of Melnik and Costa (2014) accounts for the possibility of a dual magma
298 chamber system. The model accounts for rheological changes due to volatile loss and temperature
299 driven crystallization. These processes are both effective during dome extrusion eruptions because
300 of the typical low magma ascent velocities (from millimetres to few centimetres per second), which
301 can result in magma transit times from days to weeks. These ascent times are often comparable with
302 those of crystal nucleation and growth (Melnik and Sparks, 1999; 2005; Costa et al., 2007c).

303

304 **4. Input and target data for numerical simulations**

305 4.1 Geometrical configurations of the magma plumbing system

306

307 [Within](#) the physical framework used in the Melnik and Costa (2014), the model (Fig. 1b) consists of
308 two [elastic](#) magma chambers located at different depths, with chamber pressures P_{chs} and P_{chd} able
309 to drive the magma ascent in elliptical cross-section volcanic conduit (approximating a dyke). Near
310 surface the conduit [develops](#) into a cylinder at depth L_T (named “transition level”).

311 Numerical simulations were carried out considering the shallower magma chamber (single magma
312 chamber configuration) or the double magma chamber. The single magma chamber model
313 considers a conduit feeding system composed of a shallow dyke (d_s) that connects the magma
314 chamber to a shallower cylinder, in agreement with geological and geophysical evidence from
315 different volcanoes (Melnik and Sparks, 2005; Costa et al., 2007a; Melnik et al., 2008; Melnik and
316 Costa, 2014). The double magma chamber model includes the addition of a deep reservoir
317 connected to the shallow chamber through a [deep](#) elastic dyke (d_d) (Fig. 1b).

318 In order to reproduce the observed fluctuations in discharge rates recorded in some periods of the
319 1998-2018 erupted activity, we considered a discharge rate regime where the period of pulsations is
320 controlled by the elasticity of the shallow dyke, and a discharge rate regime where the periodicity is
321 controlled by the volume of the single or dual magma chamber(s) (Barmin et al., 2002; Melnik and
322 Sparks, 2005; Costa et al., 2007a; Melnik and Costa, 2014).

323 In Appendices [A1](#) and [A2](#) we reported some test simulations in order to show the control of the
324 most sensitive parameters (i.e. water content in magma, dyke dimensions, volume of magma
325 chamber, magma influx rate into the magma chamber) affecting the model outputs in case of the
326 single magma chamber model. The volumes of the magma chamber (V_{ch}) range from 20 to 50 km³
327 and the width of the feeder dyke $2a$ from 200 to 400 m (Massaro et al., 2018a).

328 In Appendix [A3](#) is shown the sensitivity test aimed to explore a broad range of chamber volumes
329 and aspect ratios in the case of double magma chamber configuration. The deep chamber has its top
330 at 15 km of depth, it is pressurised and fed from below by a constant influx $Q_{in,d}$. The volumes of
331 shallow magma chamber (V_{chs}) range from 30 to 50 km³, and [the volumes of the deep magma](#)
332 [chamber \(\$V_{chd}\$ \)](#) from 550 to 750 km³, according to geophysical data (Cabrera-Espindola, 2010;
333 Spica et al., 2017). The aspect ratios for shallow and deep magma chambers ($AR_s - AR_d$) varied
334 from 1 to 2. For each run included in the sections 1-3 of A4, we used a fixed influx $Q_{in,d}=2.3 \text{ m}^3 \text{ s}^{-1}$,
335 and variable widths of the deeper dyke ($2a_{od}$) from 200 to 3000 m ([representative from weak to](#)
336 [strong coupling of the magma chambers; Melnik and Costa, 2014](#)). The lower dyke thickness $2b_{od}$ is
337 not an input data of the model as it changes as function of local pressure conditions, therefore it
338 does not appear in the diagrams. In Section 4 of [A3](#) we show two sets of runs having $Q_{in,d}$ equal to
339 1 and 3 m³ s⁻¹ respectively, and the following fixed parameters: AR_s and $AR_d = 1$, $V_{chd} = 650 \text{ km}^3$,
340 $V_{chs} = 40 \text{ km}^3$.

341

342 4.2 Petrological data

343

344 Erupted products at Fuego de Colima are chemically intermediate and primarily andesitic lavas with
345 ca. 61 wt.% SiO₂, (Lavallè et al., 2012). The observed dome growth phases are usually fed by
346 prolonged magma ascent times, which allow efficient degassing and crystallization. This is in
347 agreement with the low mean porosity (14-16% e.g Lavallè et al., 2012; Farquharson et al., 2015)
348 and low water contents of the products of the recent activity (2 wt. % for 1998-1999, Mora et al.,
349 2002; 0.1-2.5 wt. % for 1998-2005 products, Reubi and Blundy, 2008). Dome lava currently
350 erupted exhibits a range of crystallinities (phenocrysts, 20–30 vol.%; microlites, 25–50 vol.%), and
351 the groundmass constitutes as much as 68 vol.% (Luhr, 2002). The andesites show a porphyritic
352 texture with plagioclase (13–25 vol.%), orthopyroxene (2– 4 vol.%), clinopyroxene (3–4 vol.%) and
353 minor hornblende (<0.5%) and Fe–Ti oxides (ca. 2 vol.%). Olivine occurs rarely as xenocrysts
354 (Lavallè et al., 2012).

355 As reported in Melnik and Costa (2014), the magma viscosity μ is calculated according to Costa et
356 al. (2007a) considering the melt viscosity, μ_m , times a correction for the effects of crystallinity, θ ,
357 and for the bubbles, η . In formula:

$$358 \quad \mu = \mu_m(c, T) \theta(\beta) \eta(\alpha, Ca) \quad (2)$$

359 which depends on the melt viscosity μ_m (that is function of the water content c and temperature T),
360 on the crystal content β , on bubble fraction α and on bubble capillarity number Ca . The rheological
361 model is described in detail in Costa et al. (2007a). Table 1 summarises the value ranges used for
362 the input parameters of the model.

363

364 **5. Results**

365 In Figure 2 we showed the averages of discharge rates at Fuego de Colima volcano from November
366 1999 to October 2018. Here we define as “high” discharge rates values $> 0.1 \text{ m}^3 \text{ s}^{-1}$ (highlighted as

367 dark blue areas). All values below $> 0.1 \text{ m}^3 \text{ s}^{-1}$ are considered “low” discharge rates (light blue
368 areas). Volcanological observations are reported at the top and the bottom of the diagram. It is
369 worth noting that the “high” and “low” explosive activity correspond to the high and low discharge
370 rate, respectively. In addition, we distinguished between lava flows and lava domes accordingly to
371 the dominant emplacement style typical of each eruption, and between “low” (i.e. ash plumes, gas
372 emissions) and “high” (i.e. strong explosions, Vulcanian eruptions) magnitude explosive activity.

373 The weekly average of discharge rates represents the complete dataset used in this study, and is
374 reported in Figure 2a. These data have been calculated by using the MIROVA data (black dots) for
375 the 2000-2018 period, and complemented with published data (blue crosses) for the 1998-1999
376 period (Navarro-Ochoa et al., 2002; Zobin et al., 2005). Even if the data detection of satellite
377 thermal energy represents a continuous spectrum of information, it is worth noting that it suffers of
378 some limitations connected to cloud covering, magma composition, rheology, and emplacement of
379 the investigated lava body due to topographic conditions (Harris and Rowland, 2009; Harris et al.,
380 2010; Coppola et al., 2013). Figure 2b shows the monthly discharge rate spectrum from 1998 to
381 2018 using the MIROVA dataset (black dots), integrated with available published data (blue
382 crosses) (Navarro-Ochoa et al., 2002; Zobin et al., 2005; Capra et al., 2010; Varley et al., 2010a;
383 Sulpizio et al., 2010; James and Varley, 2012; Hutchinson et al., 2013; Reubi et al., 2013; Varley,
384 2015; Reyes-Dávila et al., 2016; Thiele et al., 2017; GVP, 2000; 2017). Figure 2c summarizes the
385 yearly average of discharge rates from MIROVA dataset, highlighting the good agreement with the
386 available average estimation of yearly discharge rates from literature (Mueller et al., 2013; Reyes-
387 Dávila et al., 2016; Aràmbula et al., 2018; GVP, 1998-2017).

388

389 5.1 Fourier analysis

390 The Fourier analysis applied to 2002-2006 period showed two periodic components, $T_0 = 24.70$ and

391 $T_1 = 6.17$ corresponding to [ca. 24](#) and [ca. 6](#) months, respectively (Appendix [A4](#) Fig. a). For 2013-
392 2016 we obtained similar results: $T_0 = 24.94$ and $T_1 = 6.23$ corresponding to [ca. 25](#) and [ca. 6](#)
393 months, respectively (Appendix [A4](#), Fig. b).

394

395 5.2 Morlet wavelet analysis

396 The whole analysed dataset is composed of 825 data points, representing the time evolution of the
397 oscillating components of the 1998-2018 eruptive activity (Fig. 2a). Figure 3a shows the normalised
398 local wavelet power spectrum of the signal. The colours scale for power values vary from light
399 orange (low values) to dark red (high values). The thick black contours represent the 95%
400 confidence level. The blue line indicates the cone of influence (COI) that delimits the region not
401 influenced by edge effects. From this analysis, it is easy to observe three main periodicities during
402 2002-2006 and 2013-2016 periods: i) long-term periodicity of ca. 1.5–2.5 years; ii) intermediate-
403 term periodicity of ca. 5-10 months; and, iii) short-term periodicity of ca. 2.5-5 weeks. The short-
404 term periodicity is also present in 2011 (Fig. 3a). Figure 3b shows the global wavelet spectrum
405 corresponding to the local wavelet power spectrum plotted in Fig. 3a. The green dashed line shows
406 the position of the best-fitting red noise model at the 95% confidence level.

407

408 5.3 Numerical simulations

409 Appendices [A1-A3](#) provide some sensitivity tests in order to explore the effects of different
410 parameters on discharge rate fluctuations for the single ([A1-A2](#)) and dual magma chamber models
411 ([A3](#)). In particular, in Appendix [A1](#) is reported the general steady-state solution of the numerical
412 model, with both stable and unstable branches (e.g. Melnik et al., 2008; Nakanishi and Koyaguchi,
413 2008), showing that the cyclic behaviour can occur only between 2 and 4 $\text{m}^3 \text{s}^{-1}$, for the fixed input
414 data (panel (a)). Varying the width of the shallow dyke $2a$ (from 200 to 400 m) and water content in

415 the melt phase, we observed how the unstable branch changes its shape. This implies different
416 periods of possible oscillations in discharge rate (panels (b)-(c)).

417 Appendix A2 provides a set of simulations carried out varying the width of the shallow dyke $2a$
418 (panel (a)). The resulting periodicities vary from ca. 1000 days ($2a = 200$ m) ca. 500 days ($2a = 300$
419 m) to ca. 250 days ($2a = 400$ m). These results highlight negative correlation between dyke widths
420 and periods of oscillation (Costa et al., 2007a). In this case, the variable widths influence the
421 intensity and periodicity of discharge rates: the wider the dyke, the lower the intensity and
422 periodicity of discharge rates. Differences in the amplitude of oscillations are observed in panel (b),
423 highlighting a positive correlation between the volume of the magma chamber V_{ch} and periodicities.
424 Periodicities of ca. 500 days correspond to 20 - 30 km³, while larger values of ca. 970 and ca. 1176
425 days are provided for 40 and 50 km³, respectively. In panel (c), we reported also a set of simulations
426 considering the modelled discharge rate controlled by the elasticity of the shallower dyke with fixed
427 influx rates Q_{in} (in the range of 0.01 - 0.1 m³ s⁻¹).

428 Appendix A3 contains [four sections dedicated to](#) the sensitivity tests for the dual magma chamber
429 model. As reported in Melnik and Costa (2014), the dual chamber model shows cyclic behaviour
430 with a period that depends on the intensity of the influx rate and the chamber connectivity
431 (described as the horizontal extent of the dyke connecting the two chambers). For a weak
432 connectivity, the overpressure in the deeper chamber remains nearly constant during the cycle and
433 the influx of fresh magma into the shallow chamber is also nearly constant. For a strong
434 connectivity between the two chambers, their overpressures increase or decrease during the cycle in
435 a synchronous way. Influx into the shallow chamber stays close to the extrusion rate at the surface
436 (Melnik and Costa, 2014). We explored different cases considering various fixed parameters as
437 follow: *i*) volumes of the shallow and deep magma chambers ($V_{chs} = 40$ km³, $V_{chd} = 650$ km³); *ii*)
438 aspect ratios ($AR_s = 1$, $AR_d = 1$) and the deep magma chamber volume ($V_{chd} = 650$ km³); *iii*) aspect
439 ratios ($AR_s = 1$, $AR_d = 1$) and the shallow magma chamber volume ($V_{chs} = 40$ km³). For *i*), *ii*) and
440 *iii*) cases, the deep influx rate $Q_{in,d}$ has fixed values from 3 to 1 m³/s. In conclusion, these

441 sensitivity tests showed the passage from weakly connected magma chambers (lack of simultaneous
442 oscillation of $Q_{in,s}$ and Q_{out}) when $2a_{od} = 200$ m to strongly connected magma chambers
443 (synchronous oscillations of $Q_{in,s}$ and Q_{out}) when $2a_{od} = 3000$ m.

444 [Figure 4 reported the results of numerical simulations aimed to reproduce the Fuego de Colima](#)
445 [fluctuations during 1998-2018.](#) Figure 4a shows a representative example of time-dependent
446 solution for a discharge rate controlled by the elasticity of the shallower dyke. Simulations were
447 carried out using fixed values of pressure (blue line) and influx rate (green line) at the source region
448 of the shallower dyke. The dyke is [ca. 6000 m long](#), it has width $2a = 400$ m and thickness $2b = 2$ m
449 and a dyke-cylinder transition at 1300 m of depth. The magma chamber volume is fixed to 30 km^3 .
450 Solutions present periodicities from 16 to 40 days in agreement with the weekly periodicities of ca.
451 38-18 days (ca. 2.5-5 weeks) derived from the wavelet analysis (Fig. 3a).

452 Figure 4b describes a representative example of the single magma chamber model simulations. We
453 set the magma feeding system composed of a dyke long 6500 m, having a width $2a = 600$ m,
454 thickness $2b = 4$ m, and a dyke-cylinder transition fixed at 1000 m of depth. The chamber has a
455 volume fixed to 30 km^3 and receives a constant $Q_{in,s} = 2.3 \text{ (m}^3 \text{ s}^{-1}\text{)}$. The transient solution is
456 accounted for the discharge rate controlled by the magma chamber volume, showing an
457 intermediate-term periodicity of ca. 220 days, in agreement with the intermediate-term periodicity
458 of ca. 146-292 days (ca. 5-10 months) obtained from the wavelet analysis (Fig. 3a).

459 Figure 4c reports a representative example of the solution obtained with the dual magma chamber
460 model in order to assess the effect of the deep chamber on the discharge rate. We fixed the volumes
461 of deep and shallow magma chamber at 40 and 650 km^3 , respectively. The shallow dyke is 6500 m
462 long with a width $2a = 260$ m and thickness $2b = 4$ m. The deep dyke has a width $2a_{od} = 500$ m, and
463 a deep influx rate $Q_{in,d} = 2.3 \text{ (m}^3 \text{ s}^{-1}\text{)}$. A cyclic behaviour of ca. 825 days is observed, reaching a
464 peak discharge rate of ca. $6 \text{ (m}^3 \text{ s}^{-1}\text{)}$. This result is in agreement with the long-term periodicity of ca.
465 547-913 days (ca. 1.5 - 2.5 years) derived from the wavelet analysis (Fig. 3a).

466 [Considering uncertainties in both modelling results and parameters and the fact that the thickness](#)

467 and width of the dykes are function of the local overpressure, results are quite consistent, although
468 with a single model configuration the current model approach cannot reproduce at the same time the
469 periodicity observed at different time scales.
470
471

472 **6. Discussions**

473 In recent years, many studies have focused on magma flow dynamics in volcanic conduits during
474 lava dome building eruptions (Melnik and Sparks, 1999; Wylie et al., 1999; Barmin et al., 2002;
475 Melnik and Sparks, 2002; 2005; Costa et al., 2007a,b; Nakanishi and Koyaguchi, 2008; Kozono and
476 Koyaguchi, 2012), highlighting periodic variations in discharge rate due to the transition from low
477 regime (allowing efficient crystals growth leading to an increase in magma viscosity) to high
478 regime (with negligible crystallization). This difference in discharge rates can be of orders of
479 magnitude, with strongly non-linear responses to the variation of governing parameters from the
480 volcanic system. This behaviour allows periodic oscillations of the discharge rate (Nakada et al.,
481 1999; Watts et al., 2002), as observed in different dome extrusion eruptions (e.g. Mt St. Helens,
482 Santiaguito, Montserrat; Melnik et al., 2008). Although each volcano usually shows its complex
483 pattern of discharge fluctuations, the cause can be explained as the superimposition of long,
484 intermediate, and short-term effects of the coupled magma chamber(s) and conduit dynamics. The
485 long-term oscillations in discharge rate are function of magma chamber size, magma
486 compressibility, and of the amount and frequency of magma recharge and withdrawal (Barmin et
487 al., 2002; Costa et al., 2007b; Melnik et al., 2008; Costa et al., 2013). The short-term and
488 intermediate oscillation dynamics can also superimpose to the main long-term periodicity, through
489 small changes in magma temperature, water content, and kinetic of crystallization during magma
490 transit in the conduit (e.g., Melnik et al., 2008). The aforementioned eruptive behaviour
491 characterized also the Fuego de Colima activity in the 1998-2018 period, as demonstrated by the
492 wavelet analysis of satellite thermal data. It is worth noting that the oscillating behaviour is not

493 regular, having a period, between 2007 and 2012, that does not show any significant periodicity
494 [\(Fig. 3a\) that may indicate a damped oscillation \(Appendix A2\)](#). During this period the volcano
495 enter in an almost quiescent status with very low discharge rates. This period of low discharge rates
496 is punctuated by low explosive activity, triggered by dome collapse or pressurization of the upper
497 conduit.

498 [It is well known for Fuego de Colima that Vulcanian explosions can evacuate significant portions of](#)
499 [the upper conduit and destroy the lava dome. The influence of these processes on the periodicity of](#)
500 [at least short-term periodic regimes could be significant. However, it is expected that these](#)
501 [processes should affect mainly sub-daily periodicities, as explained by Costa et al. \(2012\) who](#)
502 [analysed the periodicity variation due to the collapse of 200 m high plug at Montserrat, and these](#)
503 [should have a significant effects on the multi-week periodicity analysed here. Certainly, it is not](#)
504 [excluded an exceptional large evacuation of the upper conduit would be able to influence longer](#)
505 [periodicities as those investigated here.](#)

506 In order to investigate the relationship between the periodic components observed in wavelet
507 analysis and the dynamics of the Fuego de Colima feeding system, we run simulations using the
508 numerical model Melnik and Costa (2014) (Fig. 4). The model can reproduce the results of the
509 wavelet analysis in terms of observed periodicities, allows us to relate short-, intermediate- and
510 long-term oscillations in discharge rates to the dynamics of upper conduit, shallow magma
511 chamber, and coupled shallow and deep magma chambers, respectively. This implies that the
512 pressurization of the deep magma chamber has cascade effects on the whole feeding system of the
513 Fuego the Colima, similarly to what observed in other recent lava dome eruptions (i.e. Montserrat;
514 (Melnik and Costa, 2014). It is of particular interest that the best output with the dual magma
515 chamber model indicates that chambers do not oscillate simultaneously (“decoupled oscillation”;
516 Fig. 4c). Although the presented data provide, for the first time, a framework able to explain the
517 periodic behaviour of effusive activity at Fuego de Colima volcano, both numerical model and
518 wavelet analysis suffer of some limitations that need to be taken into account in interpreting the

519 results:

520 *i)* the available data of discharge rates and dome volumes collected for the 1998-2018
521 period do not have the same quality. For this reason, this lead us to extract only averages of
522 discharge rate for the entire period, with biasing effects to lower amplitudes;
523 *ii)* a common weakness of the spectral and wavelet analysis techniques is their inability to
524 distinguish the source of any given periodic component (i.e. whether it is a signal from a
525 volcanic process, an external process or if it is noise in the data). Elucidating the exact
526 mechanism requires competing robust models and multiple independent field observations
527 (Odbert and Wadge, 2009);
528 *iii)* assumptions behind the numerical model imply several limitations, such as those due to
529 the constant value of the dyke width and simplified Newtonian rheology. The first
530 assumption greatly oversimplifies the physics. In the case of large overpressures, stress at
531 the dyke tips will exceed the fracture toughness of the rocks and the dyke will expand
532 horizontally (Massaro et al., 2018b), reaching some equilibrium configuration. When the
533 deep chamber deflates, overpressure in the deeper dyke will decrease and, as flow rate
534 decreases, magma at the dyke tips can solidify, leading to a decrease in $2a_{0d}$ (Kavanagh and
535 Sparks, 2011; Melnik and Costa, 2014). Thermal exchange with wall rock can also affect
536 the nonlinear dynamics of the system (Costa and Macedonio, 2002; Melnik et al., 2008). In
537 addition, a more realistic estimate of the magma viscosity during lava dome eruptions
538 should account for the coupling with energy loss, viscous dissipation, and stick–slip effects
539 (e.g. Costa and Macedonio, 2005; Costa et al. 2007c; 2013).

540 Although this study revealed that different periodic signals are controlled by different mechanisms
541 occurring in the plumbing system, the current model approach is not able describe the three
542 periodicities (long-, intermediate- and short-term) using a unique model configuration.
543 Nevertheless, we hope that this work motivate further numerical modelling approaches in order to

544 | [develop more sophisticated models able to describe all three time scale together by incorporating](#)
545 | [further physical aspects \(e.g. full thermal effects\) and considering fully 3D geometries. .](#)

546

547 | **7. Conclusions**

548 | The coupling of wavelet analysis and numerical modelling allowed deciphering of eruptive
549 | behaviour of Fuego de Colima in the period 1998-2018, as revealed by satellite thermal data. Three
550 | periodicities emerged from the study: i) long-term ii) intermediate-term, and, iii) short-term.

551 | The long-term periodicity extracted from wavelet analysis is ca. 913-547 days (ca. 1.5-2.5 years),
552 | which can be replicated by the dual magma chamber model that provided a periodicity of ca. 1000-
553 | 500 days. The intermediate-term periodicity obtained from wavelet analysis (ca. 146-292 days, 5-10
554 | months) can be replicated by the single magma chamber model, which provides a periodicity of ca.
555 | 220 days. The short-term periodicity of ca. 18-38 days (ca. 2.5-5 weeks) is matched by model
556 | outputs considering the dynamics of the upper conduit (ca. 16-40 days). The depicted behaviour of
557 | effusive activity at Fuego de Colima is here presented for the first time, showing how the volcano
558 | presents similarities with eruptive dynamics of other recent lava dome eruptions (i.e. [SHV](#),
559 | Montserrat, Costa et al., 2013).

560

561

562 | **Code availability**

563 | Melnik and Costa (2014) code is a research software and is not still available for distribution as it
564 | lacks of documentation. It can be used by contacting the authors under their supervision.

565

566

567 | **Data availability**

568 | The original thermal dataset is available on www.mirovaweb.it. Excel worksheets can be obtained
569 | by contacting the authors.

570

571

572

573 | **Appendices**

574

575 | **Appendix A1.** Sensitivity tests for steady state solutions of discharge rate vs chamber pressure (top)
576 | and time evolution of discharge rates (bottom). These solutions are referred to the following main
577 | input parameters: i) dyke thickness $2b = 40$ m as the conduit diameter at the top ($D=2b$), the

578 transition from the dyke to cylindrical conduit $L_T = 500$ m below the surface, the length of the dyke
579 $L_d = 6$ km, and the volume of the magma chamber $V_{ch} = 50$ km³. (a) General solution showing the
580 transient regime where the periodicity can occur; (b) Solutions influenced by the dyke width $2a$
581 (from 200 to 400 m); (c) Solutions influenced by the proportion of the water content in the melt
582 (H₂O from 4 to 5 %).

583

584 **Appendix A2.** Sensitivity tests for transient solutions using the single magma chamber model. As a
585 reference these solutions have the same main input parameters used for A1. (a) Dependence of
586 discharge rate on time considering the influence of the dyke width $2a$ (from 200 to 400 m); (b)
587 Influence of the magma chamber volume V_{ch} (from 20 to 50 km³); (c) Dependence of discharge rate
588 on time considering the dyke elasticity. Each curve shows a solution with a constant influx rate Q_{in}
589 (in the range of 0.01- 0.1 m³ s⁻¹).

590

591 **Appendix A3.** Sensitivity tests for transient solutions using the dual magma chamber model. The
592 shallow feeding system has dyke with a width $2a = 200$ m, $2b = 40$ m, and $L_T = 500$ m. The
593 cylindrical conduit diameter $D = 2b$. For each diagram, is indicated the outflow (Q_{out} ; black red and
594 green lines), the flux entering into the shallower magma chamber (Q_{ins} ; blue line) and periods in
595 days (T). Runs of Section 1-2-3 have fixed $Q_{in,d} = 2.3$ (m³ s⁻¹).

596 • *Section 1)* The volumes of the shallow and deep magma chambers are fixed to 40 km³ and
597 650 km³, respectively. A set of runs is carried out for three different aspect ratios (AR) of the
598 shallow and deep chambers ($AR_s = 1$; $AR_d = 1$, $AR_s = 2$; $AR_d = 1$, $AR_s = 2$; $AR_d = 1.5$)
599 considering three widths of the deeper dyke ($2a_{0d} = 200$ m - black line, 1000 m - red line,
600 3000 m - green line).

601 • *Section 2)* The volume of the deeper magma chamber and the aspect ratios of both shallow
602 and deep chambers are fixed to 650 km³ and $AR_s = AR_d = 1$. A set of runs is provided for
603 three different shallow chamber volumes ($V_{chs} = 30$ km³, 40 km³, 50 km³) considering three
604 widths of the deeper dyke ($2a_{0d} = 200$ m - black line, 1000 m - red line, 3000 m - green
605 line);

606 • *Section 3)* The shallow chamber volume and the aspect ratios of both shallow and deep
607 chambers are fixed to 40 km³ and $AR_s = AR_d = 1$, respectively. A set of runs is carried out
608 for three deep chamber volumes ($V_{chd} = 550$ km³, 650 km³, 750 km³) considering three
609 widths of the deeper dyke ($2a_{0d} = 200$ m - black line, 1000 m - red line, 3000 m - green
610 line).

611 • Section 4) The shallow and deep chamber volumes are fixed to 40 km³ and 650 km³,

612 respectively. Two set of runs are carried out for $Q_{in,d}$ equal to 1 and 3 ($\text{m}^3 \text{s}^{-1}$). The aspect
613 ratios (AR) of the shallow and deep chambers are both equal to 1, considering three widths
614 of the deeper dyke ($2a_{od} = 200 \text{ m}$ - black line, 1000 m - red line, 3000 m - green line).

615
616
617 [Appendix A4. Results of the Fourier analysis. \(a\) The 2002-2006 period shows two main periodic](#)
618 [components, \$T_0 = 24.70\$ and \$T_1 = 6.17\$ months, corresponding to ca. 2 years and ca. 6 months,](#)
619 [respectively; \(b\) The 2013-2016 period shows similar results: \$T_0 = 24.94\$ and \$T_1 = 6.23\$ months,](#)
620 [corresponding to ca. 2.1 years and ca. 6 months, respectively.](#)

621
622
623 **Author's contribution**

624
625 SM and AC compiled the numerical simulations and formulated the adopted methodology. DC
626 provided and processed the satellite thermal data. LC provided the volcanological data. SM and RS
627 wrote the manuscript with the input of all co-authors. All authors worked on the interpretation of
628 the results.

629
630
631 **Competing interests**

632 The authors declare that they have no conflict of interest.

633 **Acknowledgments**

634
635 SM thanks Centro de Geociencias of Queretaro (UNAM, Mexico) for the hospitality during the
636 period of research at Fuego de Colima volcano, the Doctoral Course in Geoscience of University of
637 Bari (Italy) for the partial financial support and Dr. F. Loparco for the help with the Python coding.
638 LC was supported by PAPIIT-UNAM n° 105116 project. [All authors are grateful to the reviewers](#)
639 [for their valuable comments and suggestions useful to improve the manuscript.](#)

640
641
642 **References**

643
644 Arámbula-Mendoza, R., Lesage, P., Valdèz-Gonzales, C., Varley, N., Reyes-Dávila, G. and
645 Navarro-Ochoa, C.: Seismic activity that accompanied the effusive and explosive eruptions
646 during the 2004–2005 period at Volcàn de Colima, Mexico, *J. Volcanol. Geotherm. Res.*,
647 205, 30–46, 2011.

648 Arámbula-Mendoza, R., Reyes-Dávila, G., Dulce, M. V. B., González-Amezcuca, M., Navarro-
649 Ochoa, C., Martínez-Fierros, A., and Ramírez-Vázquez, A.: Seismic monitoring of
650 effusive-explosive activity and large lava dome collapses during 2013–2015 at Volcán de
651 Colima, Mexico. *J. Volcanol. Geotherm. Res.*, 351, 75-88, 2018.

652
653 Barmin, A., Melnik, O. and Sparks, R.S.J.: Periodic behavior in lava dome eruptions, Earth
654 Planet. Sci. Lett., 199 (1), 173-184, 2002.
655
656 Belousov, A., Voight, B., Belousova, M. and Petukhin, A.: Pyroclastic surges and flows from the 8-
657 10 May 1997 explosive eruption of Bezymianny volcano, Kamchatka, Russia, B. Volcanol.,
658 64 (7), 455-471, 2002.
659
660 Bernstein, M., Pavez, A., Varley, N., Whelley, P. and Calder, E.S.: Rhyolite lava dome growth
661 styles at Chaitén Volcano, Chile (2008-2009): Interpretation of thermal imagery, Andean
662 Geology, 40 (2), 2013.
663
664 Brèton-Gonzalez, M., Ramirez, J.J. and Navarro-Ochoa, C.: Summary of the historical eruptive
665 activity of Volcan de Colima, Mexico 1519-2000, J. Volcanol. Geotherm. Res., 117, 21–46,
666 2002.
667
668 Bonasia, R., Capra, L., Costa, A., Macedonio, G., and Saucedo, R.: Tephra fallout hazard
669 assessment for a Plinian eruption scenario at Volcán de Colima (Mexico), J. Volcanol.
670 Geotherm. Res., 203, 12-22, 2011.
671
672 Capra, L., Borselli, L., Varley, N., Gavilanes-Ruiz, J. C., Norini, G., Sarocchi, D., and Cortes, A.:
673 Rainfall-triggered lahars at Volcán de Colima, Mexico: surface hydro-repellency as
674 initiation process. J. Volcanol. Geotherm. Res., 189 (1-2), 105-117, 2010.
675
676 Capra, L., Macías, J.L., Cortés, A., Dávila, N., Saucedo, R., Osorio-Ocampo, S., Arce, J.L.,
677 Galvilanes-Ruiz, J.C., Corona-Càvez, P., García-Sanchez, L., Sosa-Ceballos, G., Vasquez, R.:
678 Preliminary report on the July 10–11, 2015 eruption at Volcán de Colima: Pyroclastic
679 density currents with exceptional runouts and volume, J. Volcanol. Geotherm. Res., 310,
680 39-49, 2016.
681
682 Cazelles, B., Chavez, M., Berteaux, D., Ménard, F., Vik, J. O., Jenouvrier, S., and Stenseth, N.C.:
683 Wavelet analysis of ecological time series. Oecologia, 156(2), 287-304, 2008.
684
685 Christopher, T.E., Blundy, J., Cashman, K., Cole, P., Edmonds, M., Smith, P. J., and Stinton, A.:
686 Crustal-scale degassing due to magma system destabilization and magma-gas decoupling
687 at Soufrière Hills Volcano, Montserrat. Geochem. Geophys. Geosyst., 16(9), 2797-2811,
2015.
688
689 Coppola, D., Piscopo, D., Staudacher, T. and Cigolini, C.: Lava discharge rate and effusive
690 pattern at Piton de la Fournaise from MODIS data. J. Volcanol. Geotherm. Res., 184 (1–2),
174–192, 2009.
691
692 Coppola, D., Laiolo, M., Piscopo, D. and Cigolini, C.: Rheological control on the radiant
693 density of active lava flows and domes. J. Volcanol. Geotherm. Res., 249, 39-48, 2013.
694
695 Coppola, D., Laiolo, M., Cigolini, C., Delle Donne, D., and Ripepe, M.: Enhanced volcanic hot-
696 spot detection using MODIS IR data: results from the MIROVA system. Geol. Soc.
697 London, Special Publications, 426(1), 181-205, 2016.
698 [Costa A. and Macedonio G.: Nonlinear phenomena in fluids with temperature-dependent viscosity:
699 a hysteresis model for magma flow in conduits, Geophys. Res. Lett., 29, 1402, 2002.](#)
700

- 701 Costa A. and Macedonio, G: Viscous heating in fluids with temperature-dependent viscosity:
702 Triggering of secondary flows, *J. Fluid Mech.*, 540, 21– 38, 2005.
703
- 704 Costa, A., Melnik, O., Sparks, R.S.J.: Controls of conduit geometry and wallrock elasticity on lava
705 dome eruptions, *Earth Planet. Sci. Lett.*, 260, 137–151, 2007a.
706
- 707 Costa, A., Melnik, O., Sparks R.S.J. and Voight, B.: Control of magma flow in dykes on
708 cyclic lava dome extrusion, *Geophys. Res. Lett.*, 34 (2), 2007b.
709
- 710 Costa, A., Melnik, O. and Vedeneeva, E.: Thermal effects during magma ascent in conduits, *J.*
711 *Geophys. Res.*, Vol. 112, B12205, 2007c.
712
- 713 Costa A., Caricchi L., Bagdassarov N.: A model for the rheology of particle-bearing
714 suspensions and partially molten rocks, *Geochem. Geophys. Geosyst.*, 10, Q03010,
715 doi:10.1029/2008GC002138, 2009.
716
- 717 Costa, A., Wadge, G., Melnik, O.: Cyclic extrusion of a lava dome based on a stick-slip
718 mechanism. *Earth Planet. Sci. Lett.*, 337, 39-46, 2012.
719
- 720 Costa, A., Wadge, G., Stewart, R., Odbert, H.: Coupled subdaily and multiweek cycles during the
721 lava dome eruption of Soufrière Hills Volcano, Montserrat. *J. Geophys. Res., Solid Earth*,
722 118(5), 1895-1903, 2013.
723
- 724 Clavijero, F.X.: *Historia Antigua de Mexico*, Sepan Cuantos, 29, Porrua, 1780.
725
- 726 Cortés, A., Garduño-Monroy, V.H., Navarro-Ochoa, C., Komorowski, J.C., Saucedo, R., Macías,
727 J.L. and Gavilanes, J.C.: Carta geológica del Complejo Volcánico de Colima, con
728 Geología del Complejo Volcánico de Colima, *Univer. Nat. Autón. México, Inst. Geol.,*
729 *Cartas Geológicas y Mineras*, 10, 2005.
- 730 Daubechies: *Ten Lectures on Wavelets*. Society for Industrial and Applied Mathematics, 357, 1992.
- 731 De Bélizal, É., Lavigne, J.C., Gaillard, D. Grancher, I. Pratomo, I., and Komorowski, J.C.: The
732 2007 eruption of Kelut volcano (East Java, Indonesia): phenomenology, crisis
733 management and social response, *Geomorphology*, 136(1), 165-175, 2012.
734
- 735 De la Cruz-Reyna, S.: Random patterns of activity of Colima Volcano, Mexico, *J. Volcanol.*
736 *Geotherm. Res.*, 55, 51–68, 1993.
737
- 738 | Denlinger, R.P. and Hoblitt, R.P.: Cyclic eruptive behavior of silicic volcanoes, *Geology*, 27 (5),
739 459-462 1999.
740
- 741 | Dragoni, M. and Tallarico, A.: Assumption in the evaluation of lava effusion rates from heat
742 radiation. *Geoph. Res. Lett.*, 36, L08302, 2009.
- 743 Farge, M.: Wavelet transforms and their applications to turbulence. *Annu. Rev. Fluid Mech.*, 24,
744 395–457, 1992.
- 745 Farquharson, J., Heap, M.J., Varley, N. R., Baud, P. and Reuschlé, T.: Permeability and porosity
746 relationships of edifice-forming andesites: a combined field and laboratory study. *J. Volcanol.*
747 *Geotherm. Res.*, 297, 52-68, 2015.

748
749 Fougere, P.: On the accuracy of spectrum analysis of red noise processes using maximum entropy
750 and periodogram models: simulation studies and application to geophysical data. *J.*
751 *Geophys. Res.* 90, 4355–4366, 1985.

752
753 Garel, F., Kaminski, E., Tait, S., Limare, A.: An experimental study of the surface thermal
754 signature of hot subaerial isoviscous gravity currents: implications for thermal monitoring of
755 lava flows and domes. *J. Volcanol. Geotherm. Res.*, 117, B02205, 2012.

756 Gavilanes-Ruiz, J.C., Cuevas-Muñiz, A., Varley, N., Gwynne, G., Stevenson, J., Saucedo-Girón,
757 R., and Cortés-Cortés, A.: Exploring the factors that influence the perception of risk: The
758 case of Volcán de Colima, Mexico, *J. Volcanol. Geotherm. Res.*, 186(3), 238-252, 2009.

759
760 Global Volcanism Program: Report on Colima (Mexico). In: Wunderman, R (ed.), *B. Global*
761 *Volcanism Net.*, 23-10, Smithsonian Institution, 1998.

762
763 Global Volcanism Program: Report on Colima (Mexico). In: Wunderman, R (ed.), *Bulletin of the*
764 *Global Volcanism Network*, 25-6, Smithsonian Institution, 2000.

765
766 Global Volcanism Program: Report on Colima (Mexico). In: Wunderman, R (ed.), *B. Global*
767 *Volcanism Net.*, 27-11, Smithsonian Institution, 2002.

768
769 Global Volcanism Program: Report on Colima (Mexico). In: Venzke, E (ed.), *B. Global*
770 *Volcanism Net.*, 28-11, Smithsonian Institution, 2003.

771
772 Global Volcanism Program: Report on Colima (Mexico). In: Wunderman, R (ed.), *B. Global*
773 *Volcanism Net.*, 38-12, Smithsonian Institution, 2013.

774
775 Global Volcanism Program: Report on Colima (Mexico). In: Sennert, S K (ed.), *Weekly Volcanic*
776 *Activity Report*, 26 July-1 August 2017, Smithsonian Institution and US Geological Survey,
777 2017.

778
779 Harris, A.J., Rose, W.I. and Flynn, L.P.: Temporal trends in lava dome extrusion at Santiaguito
780 1922-2000, *B. Volcanol.*, 65(2), 77-89, 2003.

781
782 Harris, A.J.L., Rowland, S.K.: Effusion rate controls on lava flow length and the role of heat
783 loss: a review. In: Thordarson, T., Self, S., Larsen, G., Rowland, S.K., Hoskuldsson, A.
784 (Eds.), *Studies in Volcanology: The Legacy of George Walker: Special Publication*
785 *IAVCEI*, 2, pp. 33–51, 2009.

786
787 Harris, A.J.L., Favalli, M., Steffke, A., Fornaciai, A., Boschi, E.: A relation between lava
788 discharge rate, thermal insulation, and flow area set using lidar data. *Geoph. Res.*
Lett., 37, L20308. <http://dx.doi.org/10.1029/2010GL044683>, 2010.

789
790 Heap, M.J., Lavallée, Y., Petrakova, L., Baud, P., Reuschle, T., Varley, N., and Dingwell D.B.:
791 Microstructural controls on the physical and mechanical properties of edifice-forming
792 andesites at Volcán de Colima, Mexico, *Solid Earth*, 119 (4), 2925-2963, 2014.

793
794 Hutchison, W., Varley, N., Pyle, D.M., Mather, T.A., and Stevenson, J.A.: Airborne thermal
795 remote sensing of the Volcán de Colima (Mexico) lava dome from 2007 to 2010, *Geol. Soc.*
London, Spec. Public., 380 (1), 203-228, 2013.

796
797 James, M. R. and Varley, N.: Identification of structural controls in an active lava dome with high
798 resolution DEMs: Volcán de Colima, Mexico. *Geoph. Res.Lett.*, 39(22), 2012.
799
800 Kavanagh, J. L. and Sparks, R.S.J.: Insights of dyke emplacement mechanics from detailed 3D dyke
801 thickness datasets. *J.Geol. Soc.*, 168(4), 965-978, 2011.
802
803 [Kozono, T. and Koyaguchi, T.: Effects of relative motion between gas and liquid on 1-dimensional](#)
804 [steady flow in silicic volcanic conduits: 2. Origin of diversity of eruption styles. *J.*](#)
805 [Volcanol. Geotherm. Res, 180\(1\), 37-49, 2009.](#)
806
807 Kozono, T. and Koyaguchi, T.: Effects of gas escape and crystallization on the complexity of
808 conduit flow dynamics during lava dome eruptions. *Geoph. Res.Lett.*, Solid Earth, 117(B8),
809 2012.
810
811 Lamb, O.D., Varley, N., Mather, T.A., Pyle, D.M., Smith, P.J. and Liu, E.J.: Multiple timescales of
812 cyclical behaviour observed at two dome-forming eruptions, *J. Volcanol. Geotherm. Res.*,
813 284, 106-121, 2014.
814
815 Lau K.M. and Weng H.: Climatic signal detection using wavelet transform: how to make a time
816 series sing. *Bull Am Meteorol Soc.*, 76. 2391–2402, 1995.

817 Lavallée, Y., Varley, N., Alatorre-Ibargüengoitia, M.A., Hess, K.U., Kueppers, U., Mueller, S.,
818 Richard, D., Scheu, B., Spieler, O. and D.B. Dingwell, D.B.: Magmatic architecture of
819 dome-building eruptions at Volcan de Colima (Mexico), *Bull. Volcanol.*, 74 (1), 249-260,
820 2012.
821
822 Lensky, N.G., Navon, O. and Lyakhovsky, V.: Bubble growth during decompression of magma:
823 experimental and theoretical investigation, *J. Volcanol. Geotherm. Res.*, 129 (1), 7-22, 2004.
824
825 Loughlin, S.C., Luckett, R., Ryan, G., Christopher, T., Hards, V., De Angelis, S. and Strutt, M.:An
826 overview of lava dome evolution, dome collapse and cyclicity at Soufrière Hills Volcano,
827 Montserrat, 2005–2007, *Geophys. Res. Lett.*, 37 (19), 2010.
828
829 Luhr, J.F. and Carmichael, I.S.: The Colima Volcanic Complex, Mexico, *Con.to Mineral.Petrol.*, 71
830 (4), 343-372, 1980.
831
832 Luhr, J.F.: Petrology and geochemistry of the 1991 and 1998-1999 lava flows from Volcan
833 Colima, Mexico, *J. Volcanol. Geotherm. Res.*, 117, 169–194, 2002.
834
835 Macias, J., Arce, J., Sosa, G., Gardner, J.E., Saucedo, R.:Storage conditions and magma
836 processes triggering the 1818CE Plinian eruption of Volcán de Colima, *J. Volcanol.*
837 *Geotherm. Res.*, doi:10.1016/j.jvolgeores.2017.02.025, 2017.

838 Mallat, S.: *A wavelet tour of signal processing*. Academic Press, San Diego, 1998.

839 Massaro, S., Sulpizio, R., Costa, A., Capra, L., Lucchi, F.: Understanding eruptive style variations
840 at calc-alkaline volcanoes: the 1913 eruption of Fuego de Colima volcano (Mexico), *B.*
841 *Volcanol*, 80-62, <https://doi.org/10.1007/s00445-018-1235-z>, 2018a.

- 842 Massaro, S., Costa, A., Sulpizio, R.: Time evolution of a magma feeding system during a Plinian
843 eruption: the example of the Pomici di Avellino eruption of Somma-Vesuvius (Italy), *Earth*
844 *Planet. Sci. Lett.* 482, 545-555, 2018b.
- 845
- 846 Medina-Martinez, F.: Analysis of the eruptive history of the Volcán de Colima, Mexico (1560–
847 1980), *Geofisica Internacional*, 22, 157–178, 1983.
- 848
- 849 Martin del Pozzo, A.L., Sheridan, M., Barrera, D., Lugo Hubp, J. and Vázquez Selem, L.:
850 Potential hazards from Colima volcano, Mexico, *Geofisica Internacional*, 34 (4), 363-376.
851 1995.
- 852
- 853 Melnik, O. and Sparks, R.S.J.: Nonlinear dynamics of lava dome extrusion, *Nature*, 402
854 (6757), 37-41, 1999.
- 855
- 856 Melnik, O. and Sparks, R.S.J: Dynamics of magma ascent and lava extrusion at Soufrière
857 Hills Volcano, Montserrat, *Geol. Soc. London Mem.*, 21 (1), 153-171, 2002.
- 858
- 859 Melnik, O. and Sparks, R.S.J: Controls on conduit magma flow dynamics during lava-dome
860 building eruptions, *J. Geophys. Res.*, 110, B02209, doi:10.1029/2004JB003183, 2005.
- 861 Melnik, O., Sparks, R.S.J., Costa, A. and Barmin, A.: (2008), *Volcanic Eruptions: Cyclicity during*
862 *Lava Dome Growth*, in Meyers: *Encyclopedia of Complexity and Systems Science*, 2008.
- 863
- 864 Melnik, O. and A. Costa, A: Dual-chamber-conduit models of non-linear dynamics behaviour at
865 Soufrière Hills Volcano, Montserrat, *Geol. Soc. Lond., Mem.*, 39, 61-69, 2014.
- 866
- 867 Mériaux, C. and Jaupart, C: Simple fluid dynamic models of volcanic rift zones, *Earth Planet. Sci.*
868 *Lett.*, 136(3-4), 223-240, 1995.
- 869
- 870 Mora, J. C., Macias, J. L., Saucedo, R., Orlando, A., Manetti, P., and Vaselli, O.: Petrology of the
871 1998–2000 products of Volcán de Colima, México. *J. Volcanol. Geotherm. Res.*, 117(1),
872 195-212, 2002.
- 873
- 874 Mueller, S.B., Varley, N., Kueppers, U., Lesage, P. and Reyes-Dávila, G.: Quantification of
875 magma ascent rate through rockfall monitoring at the growing/collapsing lava dome of
876 Volcan de Colima, Mexico, *Solid Earth*, 4, 201-213, 2013.
- 877
- 878 Nakanishi, M. and Koyaguchi, T.: A stability analysis of a conduit flow model for lava dome
879 eruptions. *J. Volcanol. Geotherm. Res.*, 178(1), 46-57, 2008.
- 880
- 881 Nakada, S., Shimizu, H. and Ohta, K.: Overview of the 1990–1995 eruption at Unzen Volcano, *J.*
882 *Volcanol. Geotherm. Res.*, 89 (1), 1-22, 1999.
- 883
- 884 Navarro-Ochoa, C., Gavilanes-Ruiz, A. Cortès-Cortès, A.: Movement and emplacement of lava
885 flows at Volcán de Colima, México: November 1998–February 1999, *J. Volcanol.*
886 *Geotherm. Res.*, 117 (1), 155-167, 2002.
- 887
- 888 Nicholson, R.S., Gardner, J.E., and Neal, C.A.: Variations in eruption style during the 1931 A.D.
eruption of Aniakchak volcano, Alaska, *J. Volcanol. Geotherm. Res.*, 207, 69–82, 2011.
- 889
- 889 Norini, G., Capra, L., Gropelli, G., Agliardi, F., Pola, A., and Cortès, A.: Structural architecture of

890 the Colima Volcanic Complex, *J. Geophys. Res.*, 115, B12209, 2010.

891

892 Odbert, H.M. and Wadge, G.: Time series analysis of lava flux. *J. Volcanol. Geotherm. Res.*,

893 188(4), 305-314, 2009.

894

895 Ozerov, A., Ispolatov, I. and Lees, J.: Modeling strombolian eruptions of Karymsky volcano,

896 Kamchatka, Russia, *J. Volcanol. Geotherm. Res.*, 122 (3), 265-280, 2003.

897

898 Ramsey, M.S. and Harris, A.J.L.: Volcanology 2020: how will thermal remote sensing of

899 volcanic surface activity evolve over the next decade? *J. Volcanol. Geotherm. Res.*,

900 <http://dx.doi.org/10.1016/j.jvolgeores.2012.05.011>, 2012.

901 Reyes-Dávila, G.A., Arámbula-Mendoza, R., Espinasa-Pereña, P., Pankhurst, M.J., Navarro-

902 Ochoa, C., Savov, I. and Domínguez-Reyes, T.: Volcán de Colima dome collapse of

903 July, 2015 and associated pyroclastic density currents, *J. Volcanol. Geotherm. Res.*, 320,

904 100-106, 2016.

905

906 Reubi, O. and Blundy, J.: Assimilation of Plutonic roots, formation of high-K exotic melt

907 inclusions and genesis of andesitic magmas at Volcán De Colima, Mexico, *J. Petrol.* 49, 12,

908 2221–2243, 2008.

909

910 Reubi, O., Blundy, J. and Varley, N.: Volatiles contents, degassing and crystallisation of

911 intermediate magmas at Volcán de Colima, Mexico, inferred from melt inclusions.

912 *Contr. Mineral. Petrol.*, 165(6), 1087-1106, 2013.

913

914 Reubi, O., Sims, K.W., Varley, N., Reagan, M. and Eikenberg, J.: Timescales of degassing and

915 conduit dynamics inferred from 210Pb–226Ra disequilibria in Volcán de Colima 1998–

916 2010 andesitic magmas. *Geol. Soc., London, Sp. Publ.*, 422, SP422-5, 2015.

917 [Roverato, M., Capra, L., Sulpizio, R., Norini, G.: Stratigraphic reconstruction of two debris](#)

918 [avalanche deposits at Colima Volcano \(Mexico\): insights into pre-failure conditions and](#)

919 [climate influence. *Journal of Volcanology and Geothermal Research*, 207\(1-2\), 33-46, 2011.](#)

920

921 Salzer, J.T., Nikkhoo, M., Walter, T.R., Sudhaus, H., Reyes-Dávila, G., Bretón, M. and Arámbula,

922 R.: Satellite radar data reveal short-term pre-explosive displacements and a complex conduit

923 system at Volcán de Colima, Mexico, *Frontiers in Earth Sci.*, 2, 12, 2014.

924

925 Saucedo, R., Macías, J.L., Sheridan, M.F., Bursik, M.I., Komorowski, J.C.: Modeling of

926 pyroclastic flows of Colima Volcano, Mexico: implications for hazard assessment, *J.*

927 *Volcanol. Geotherm. Res.*, 139 (1–2), 103–115, 2005.

928

929 Saucedo, R., J.L. Macías, J.C. Gavilanes, J.L. Arce, J.C. Komorowski, J.E. Gardner, and G.

930 Valdez-Moreno, G.: Eyewitness, stratigraphy, chemistry, and eruptive dynamics of the

931 1913 Plinian eruption of Volcán de Colima, México, *J. Volcanol. Geotherm. Res.*, 191(3),

932 149-166, 2010.

933

934 Savov, I.P., Luhr, J.F. and Navarro-Ochoa, C.; Petrology and geochemistry of lava and ash

935 erupted from Volcan Colima, Mexico, during 1998-2005, *J. Volcanol. Geotherm. Res.*, 174,

936 241–256, 2008.

937

- 938 Siswowidjoyo, S., Suryo, I. and Yokoyama, I.: Magma eruption rates of Merapi volcano,
939 Central Java, Indonesia during one century (1890–1992), *B. Volcanol.*, 57 (2), 111-116,
940 1995.
- 941
- 942 Sparks, R.S.J.: Causes and consequences of pressurisation in lava dome eruptions, *Earth Planet. Sci.*
943 *Lett.*, 150 (3-4), 177-189, 1997.
- 944
- 945 Sparks, R.S.J. and Young, S.R.: The eruption of Soufrière Hills volcano, Montserrat (1995–1999):
946 Overview of scientific results, in *The Eruption of the Soufrière Hills Volcano, Montserrat*
947 *from 1995 to 1999*, *Geol. Soc. London Mem.*, 21, 45–69, 2002.
- 948
- 949 Spica, Z., Pertou, M. and Legrand, D.: Anatomy of the Colima volcano magmatic system,
950 Mexico, *Earth Planet. Sci. Lett.*, 459, 1-13, 2017.
- 951
- 952 Sulpizio, R., Capra, L., Sarocchi, D., Saucedo, R., Gavilanes-Ruiz, J. C. and Varley, N.: Predicting
953 the block-and-ash flow inundation areas at Volcán de Colima (Colima, Mexico) based on
954 the present day (February 2010) status. *J. Volcanol. Geotherm. Res.*, 193(1-2), 49-66, 2010.
- 955
- 956 Swanson, D.A. and Holcomb, R.T.: Regularities in growth of the Mount St. Helens dacite
957 dome, 1980–1986, in *Lava Flows and Domes: Emplacement Mechanisms and Hazard*
958 *Implications*, 3-24, 1990.
- 959
- 960 Thiele, S.T., Varley, N. and James, M.R.: Thermal photogrammetric imaging: A new technique for
961 monitoring dome eruptions, *J. Volcanol. Geotherm. Res.*, 337, 140-145, 2017.
- 962
- 963 Trauth, M.: *MATLAB Recipes for Earth Sciences*, 1st ed. Springer-Verlag, Berlin Heidelberg,
964 2006.
- 965
- 966 Torrence, C. and Compo, G.P.: A practical guide to wavelet analysis. *Bulletin of the American*
967 *Meteorological society*, 79(1), 61-78, 1998.
- 968
- 969 Varley, N., Arámbula-Mendoza, R., Reyes-Dávila, G., Stevenson, J., Harwood, R.: Long-
970 period seismicity during magma movement at Volcán de Colima, *B. Volcanol.*, 72, 1093–
971 1107. <http://dx.doi.org/10.1007/s00445-010-0390-7>, 2010a.
- 972
- 973 Varley, N., Arámbula-Mendoza, R., Reyes-Reyes-Dávila, G., Sanderson, R., Stevenson, J.:
974 Generation of Vulcanian activity and long-period seismicity at Volcan de Colima, Mexico.
J. Volcanol. Geotherm. Res., 198, 45–56, 2010b.
- 975
- 976 Varley, N: *La evolución de la actividad reciente del Volcán de Colima*, webseminar, Unión
977 *Geofísica Mexicana A.C.*, 2015.
- 978
- 979 Vila, J., Macià, R., Kumar, D., Ortiz, R., Moreno, H., Correig, A.: Analysis of the unrest of active
980 volcanoes using variations of the base level noise seismic spectrum. *J. Volcanol. Geotherm.*
Res. 153, 11–20, 2006.
- 981
- 982 Voight, B., Hoblitt, R.P., Clarke, A.B., Lockhart, A. Miller, L. Lynch and McMahon, J.:
983 Remarkable cyclic ground deformation monitored in real-time on Montserrat, and its use
984 in eruption forecasting, *Geophys. Res. Lett.*, 25 (18), 3405-3408, 1998.

985 Voight, B., Sparks, R.S.J., Miller, A.D., Stewart, R.C., Hoblitt, R.P., Clarke, A. and Cole, P.:
986 Magma flow instability and cyclic activity at Soufriere Hills volcano, Montserrat,
987 british west indies, *Science*, 283 (5405), 1138-1142, 1999.
988

989 Voight, B., Constantine, E.K., Siswamidjyo, S. and Torley, R.: Historical eruptions of Merapi
990 volcano, central Java, Indonesia, 1768–1998, *J. Volcanol. Geotherm. Res.*, 100 (1), 69-138,
991 2000.
992

993 Wadge, G., Dorta, D.O. and Cole, P.D.: The magma budget of Volcán Arenal, Costa Rica
994 from 1980 to 2004, *J. Volcanol. Geotherm. Res.*, 157 (1), 60-74, 2006.
995

996 Wadge, G., Herd, R., Ryan, G., Calder, E.S. and Komorowski, J.C.: Lava production at Soufrière
997 Hills Volcano, Montserrat: 1995–2009, *Geophys. Res. Lett.*, 37 (19), 2010.
998

999 Watts, R.B., Herd, R.A., Sparks, R.S.J. and Young, S.R.: Growth patterns and emplacement of the
L000 andesitic lava dome at Soufriere Hills Volcano, Montserrat, *Geol. Soc. Lond. Mem.* 21(1),
L001 115-152, 2002.
L002

L003 Weng, H. and Lau, K.M.: Wavelets, period doubling, and time-frequency localization with
L004 application to organization of convection over the tropical western Pacific. *J. Atmos. Sci.*,
L005 51, 2523–2541, 1994.

L006 Wolpert, R., Ogburn, L. and Calder, E.S.: The longevity of lava dome eruptions. *Journal of*
L007 *Geophysical Research: Solid Earth*, 121(2), 676-686, 2016.
L008

L009 Wylie, J.J., Voight, B. and Whitehead, J.A.: Instability of magma flow from volatile dependent
L010 viscosity, *Science*, 285, 1883–1885 1999.

L011 Zobin, V.M., Orozco-Rojas, J., Reyes-Dávila, G.A. and Navarro-Ochoa, C.: Seismicity of an
L012 andesitic volcano during block-lava effusion: Volcán de Colima, México, November 1998–
L013 January 1999, *Bull. Volcanol.* 67 (7), 679-688, 2005.
L014

L015 Zobin, V.M., Varley, N., González, M., Orozco, J., Reyes, G.A., Navarro-Ochoa, C. and M.
L016 Bretón: Monitoring the 2004 andesitic block-lava extrusion at Volcán de Colima,
L017 México from seismic activity and SO₂ emission, *J. Volcanol. Geotherm. Res.*, 177 (2), 367-
L018 377, 2008.
L019

L020 Zobin, V.M., R. Arámbula, R., Bretón, M., Reyes, G., I. Plascencia, I., Navarro-Ochoa, C. and
L021 Martínez, A.: Dynamics of the January 2013–June 2014 explosive-effusive episode in the
L022 eruption of Volcán de Colima, México: insights from seismic and video monitoring, *Bull.*
L023 *Volcanol.* 77(4), 31, 2015.
L024
L025
L026
L027
L028
L029
L030
L031
L032
L033
L034

Table 1: Input parameters used in numerical simulations.

Notation	Description	Value
c_o	Concentration of dissolved gas (wt.%)	5-6
C_f	Solubility coefficient ($\text{Pa}^{-1/2}$)	4.1×10^{-6}
C_m	Specific heat ($\text{J kg}^{-1} \text{K}^{-1}$)	1.2×10^3
I_0	Max nucleation rate ($\text{m}^{-3} \text{s}^{-1}$)	3×10^{10}
L_*	Latent heat of crystallization (J kg^{-1})	3.5×10^5
μ_g	Gas viscosity (Pa s)	1.5×10^{-5}
ρ_m	Density of the melt phase (kg m^{-3})	2300-2500
ρ_c	Density of the crystal (kg m^{-3})	2700-2800
T_{ch}	Magma chamber temperature (K)	1150
P_{ch}	Magma chamber pressure (MPa)	130 – 210
β_{ch*}	Magma chamber crystal content	0.35-0.45
μ	Magma viscosity (Pa s)	3.7×10^5
ρ_r	Host rock density (kg m^{-3})	2600
G	Host rock rigidity (GPa)	6
ν	Poisson's ratio	0.25
ε		8.6
<i>Conduit geometry parameters using a single magma chamber model</i>		
D	Diameter of the cylindrical conduit	30-40
L_T	Dyke-cylinder transition depth (m)	1300-500
$2a$	Dyke width (m)	200 – 600
$2b$	Dyke thickness (m)	4-40
L	Magma chamber depth (top) (m)	6000-6500
V_{ch}	Magma chamber volume (km^3)	20-50
AR	Magma chamber aspect ratio	1-2
$Q_{in,s}$	Influx into the shallow magma chamber ($\text{m}^3 \text{s}^{-1}$)	0.01-3.5
<i>Parameters used for simulations carried out with dual magma chamber model</i>		
<i>Deep magma chamber</i>		
$2a_{od}$	Deeper dyke width (m)	200 – 3000
L_0	Deep magma chamber depth (top) (m)	15000
AR_d	Deep magma chamber aspect ratio	1-2
V_{chd}	Deep magma chamber volume (km^3)	550-750
ΔP	Deep magma chamber overpressure (MPa)	20
$Q_{in,d}$	Influx into the shallow magma chamber ($\text{m}^3 \text{s}^{-1}$)	1-3

L037 **Figures Captions**

L038 **Fig. 1.** (a) Digital elevation model of the Colima Volcanic Complex (NC = Nevado de Colima
L039 volcanso; FC = Fuego de Colima volcanso) and Colima Rift with the main tectonic and volcano-
L040 tectonic structures (modified from Norini et al. 2010). In the inset, the location of the Colima
L041 Volcanic Complex (CVC) within the Trans-Mexican Volcanic Belt (TMVB) is shown in the frame
L042 of the subduction-type geodynamic setting of Central America. (b) Schematic view of the conduit
L043 feeding system framework used for numerical simulations (modified after Melnik and Costa, 2014).

L044 **Fig. 2.** Dataset about the averaged discharge rates of Fuego de Colima during 1998-2018, derived
L045 by the MIROVA thermal data (black points) and published data (blue crosses) (Navarro-Ochoa et
L046 al., 2002; Zobin et al., 2005; Reubi et al 2013; Mueller et al., 2013; Varley, 2015; Reyes-Dávila et
L047 al., 2016; Thiele et al., 2017; GVP, 2002-2017). Values $> 0.1 \text{ (m}^3 \text{ s}^{-1}\text{)}$ are considered to be as “high”
L048 (dark blue area) and values $< 0.1 \text{ (m}^3 \text{ s}^{-1}\text{)}$ as “low” discharge rate (light blue area). The $0.01 \text{ (m}^3 \text{ s}^{-1}\text{)}$
L049 is the threshold under which the MIROVA system does not provide reliable data (blue line); (a)
L050 Weekly average discharge rates. The boxes contain symbols of volcanological observations
L051 reported in literature; (b) Monthly average discharge rates; (c) Yearly average discharge rates.

L052 **Fig. 3.** (a) Local wavelet power spectrum normalized by $1/\sigma^2$ (σ^2 in $(\text{m}^3 \text{ s}^{-1})^2$). The left axis is the
L053 period (in years). The bottom axis is time (in years). The shaded contours are at normalized
L054 variances of 0.5, 1, 2, and 4 $(\text{m}^3 \text{ s}^{-1})^2$. The black thick contour encloses regions of greater than 95%
L055 confidence for a red-noise process with a lag-1 coefficient of 0.72. It shows three orders of
L056 periodicities of: long-term (ca. 1.5-2.5 years), intermediate-term (ca. 5-10 months) during 2002-
L057 2006 and 2013-2016, and short-term (ca. 2.5-5 weeks) during 2001-2006 and 2011-2016. Blue line
L058 indicates the “cone of influence” where edge effects become important outside it; (b) Global
L059 wavelet power spectrum. The green dotted line represents the best-fitting red noise spectrum at the
L060 95% confidence level.

L061 **Fig. 4.** Results of numerical simulations. The physical framework of the conduit feeding system has
L062 deep and shallow chambers connected to surface via vertical elastic dykes evolving into non-elastic
L063 cylinder. The length of the shallow dyke L_{ds} is in the range of 6000-6500 m. The passage to cylinder
L064 conduit L_r occurs at ca. 1300-500 m below the cone. (a) Discharge rates vs. time considering the
L065 elasticity of the shallower dyke, with a width $2a = 400$ m and thickness $2b = 2$ m. The cylinder
L066 diameter $D = 30$ m. Two cases are shown: *i*) constant pressure (blue line) and *ii*) constant influx rate
L067 at the source region of the dyke, providing different periodicities of 16 and 40 days, in good

L068 agreement with the short-term (weekly) periodicities observed in Fig. 3a; (b) Discharge rate vs. time
L069 using the single magma chamber model. The dyke width $2a = 600$ and thickness $2b = 4$ m. The
L070 chamber has a volume $V_{ch} = 30 \text{ km}^3$, receiving a constant influx $Q_{in,s} = 2.3 \text{ (m}^3 \text{ s}^{-1}\text{)}$; Periodicity is of
L071 ca. 220 days, in good agreement with the intermediate-term (monthly) periodicities observed in Fig.
L072 3a; (c) Discharge rate vs. time using the dual magma chamber model. The aspect ratio of the
L073 shallow and deep chambers ($AR_s - AR_d$) are both equal to 1.3 and 1.4, respectively. The upper
L074 feeding system has a chamber ($V_{chs} = 30 \text{ km}^3$) connected to a dyke (width $2a = 260$ m; $2b = 4$ m)
L075 evolving into a cylinder ($D = 30$ m) at $L_T = 1000$ m. The shallow chamber is connected to the deep
L076 one ($V_{chd} = 500 \text{ km}^3$) through a feeder dyke ($2a_{od} = 500$ m). A constant $Q_{in,d} = 2.3 \text{ (m}^3 \text{ s}^{-1}\text{)}$ is
L077 injected from below. Periodicity is in the range of ca. 825 days, in good agreement with the long-
L078 term (yearly) periodicities observed in Fig. 3a.

L079

L080

L081

L082

L083

L084

L085

L086

L087

L088

L089

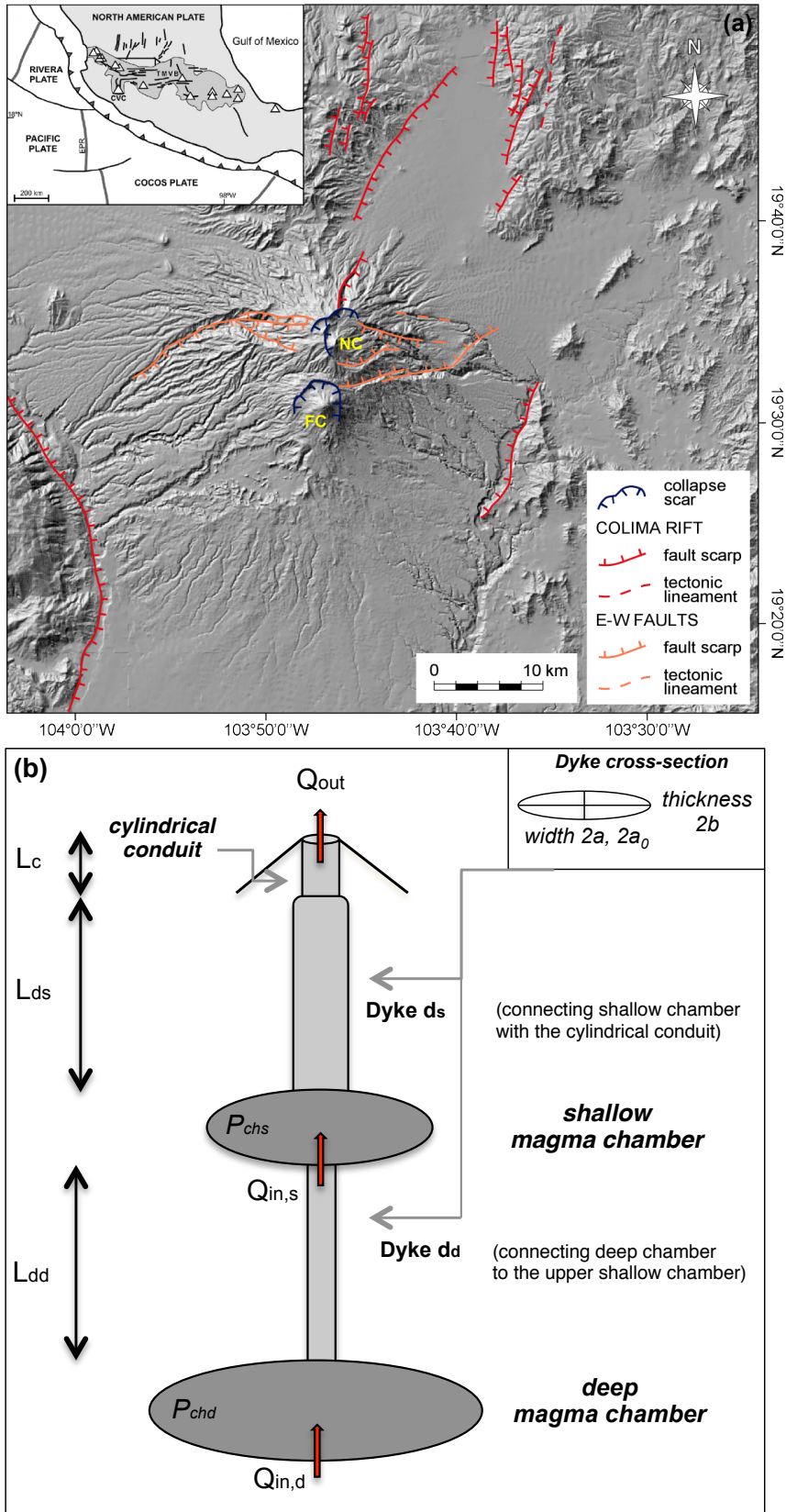
L090

L091

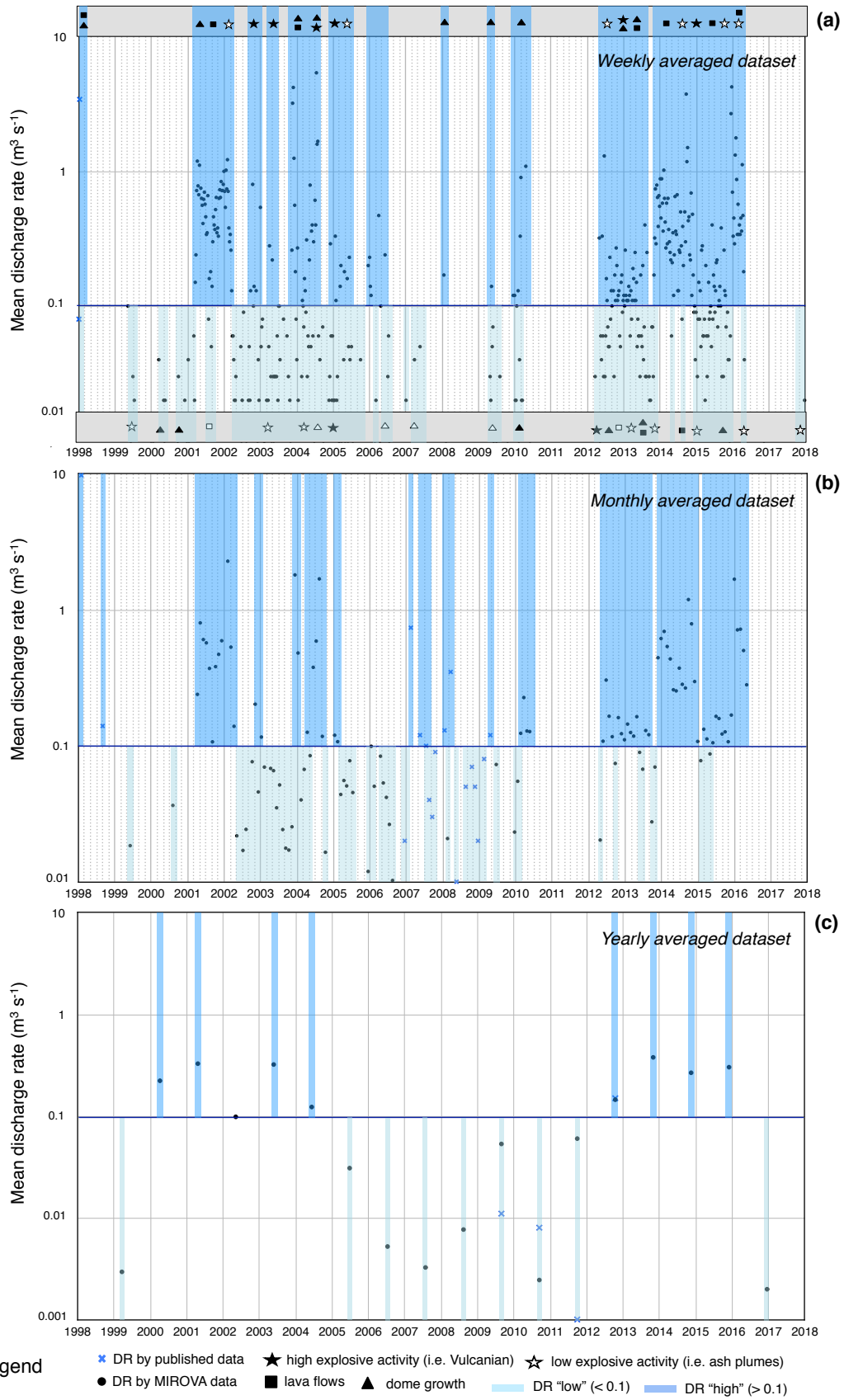
L092

L093

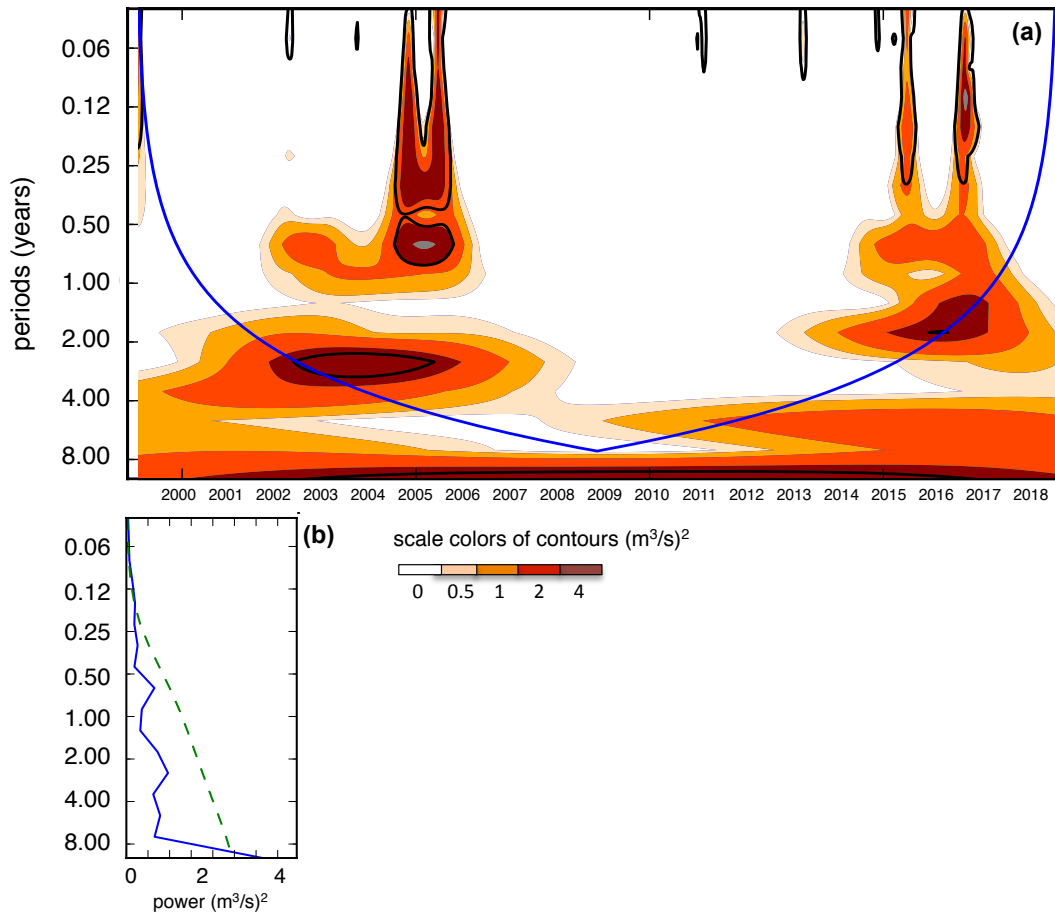
L094 Fig.1



L095



L099 **Fig.3**



L100

L101

L102

L103

L104

L105

L106

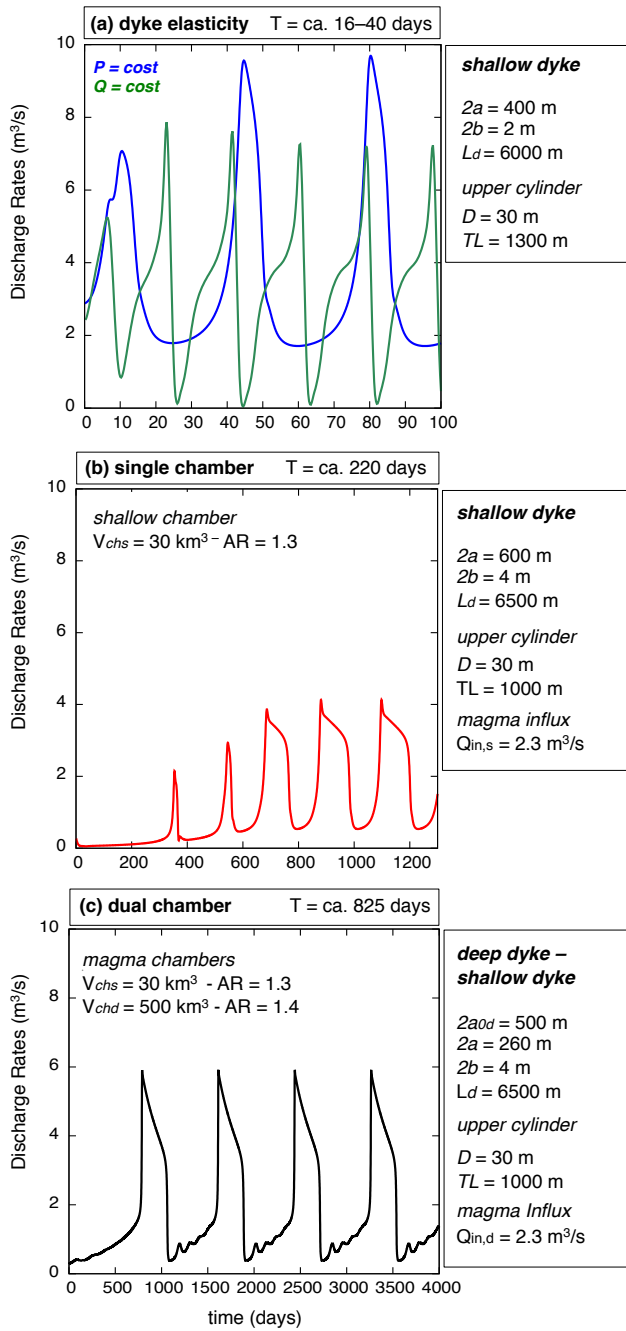
L107

L108

L109

L110

L111 Fig. 4

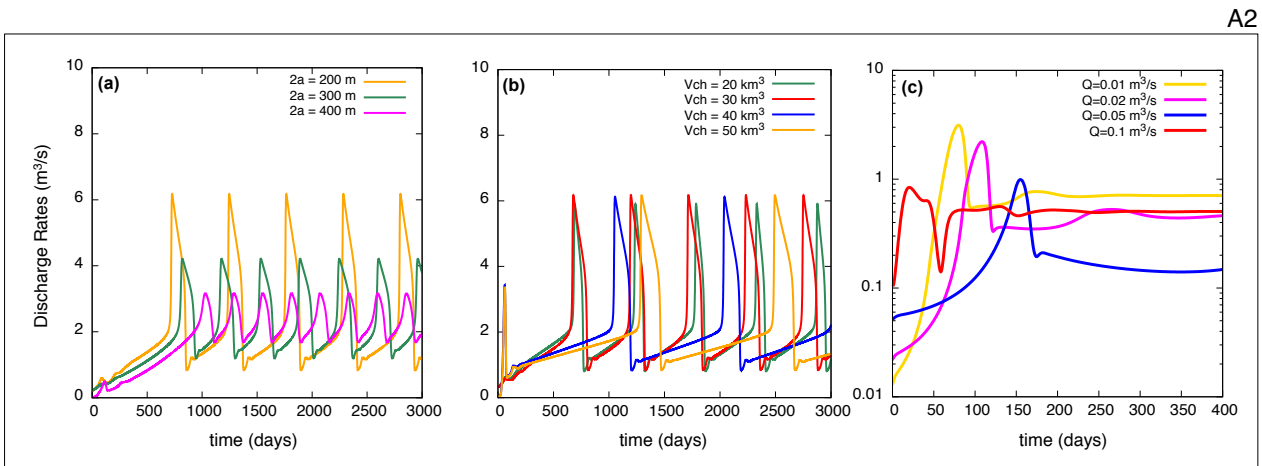
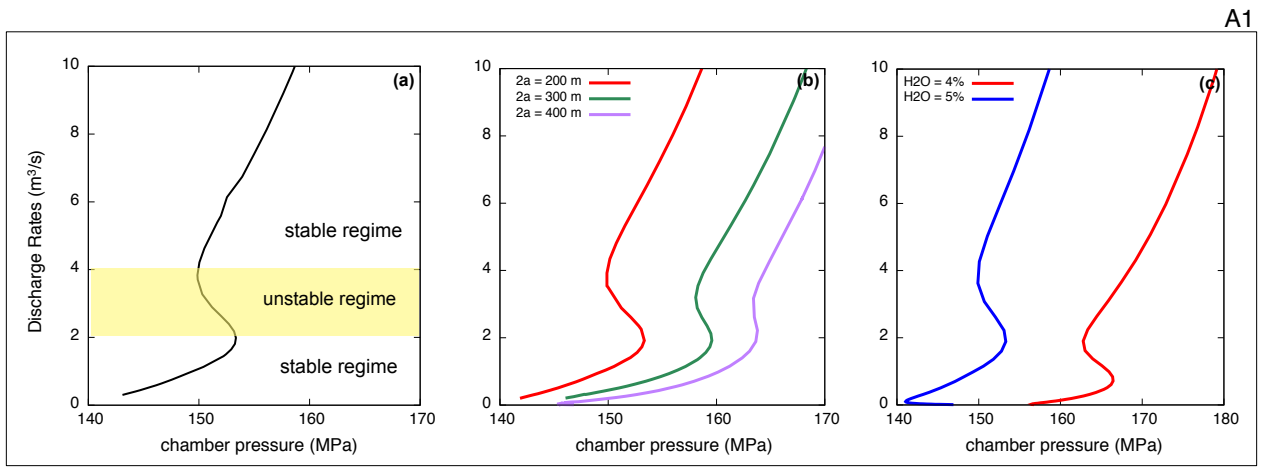


L112

L113

L114 Appendix A1-A2

L115



L116

L117

L118

L119

L120

L121

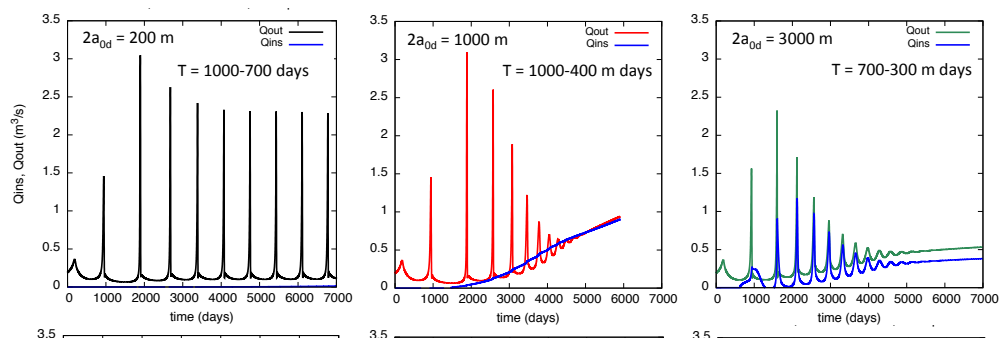
L122

L123

L124

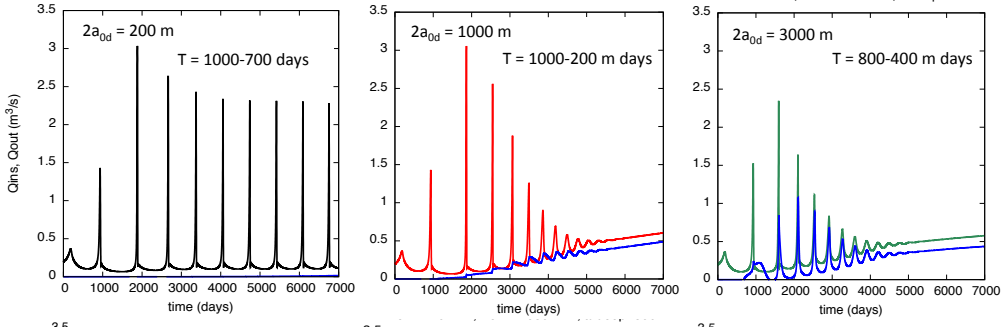
Fixed parameters
 $V_{chs} = 40 \text{ km}^3$
 $V_{chd} = 650 \text{ km}^3$

Aspect Ratio
 $ARs = 1$
 $ARd = 1$

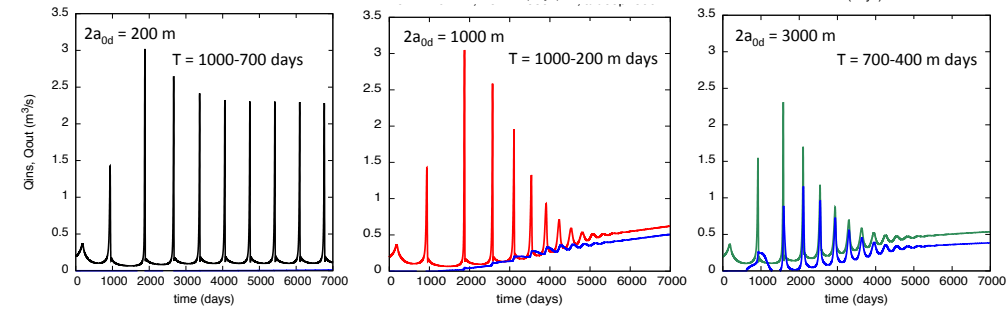


1

Aspect Ratio
 $ARs = 2$
 $ARd = 1$

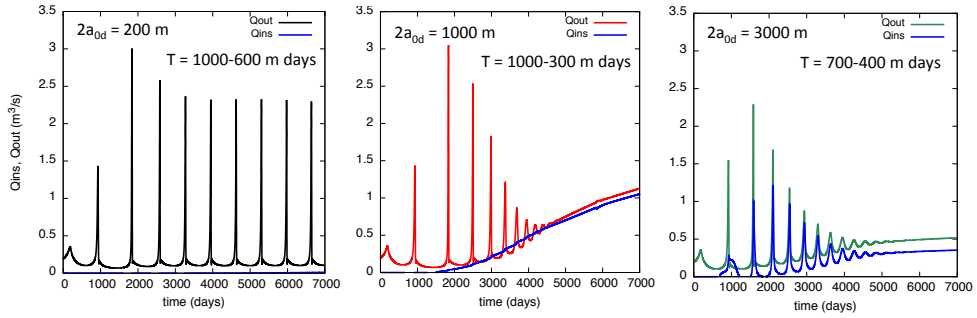


Aspect Ratio
 $ARs = 2$
 $ARd = 1.5$

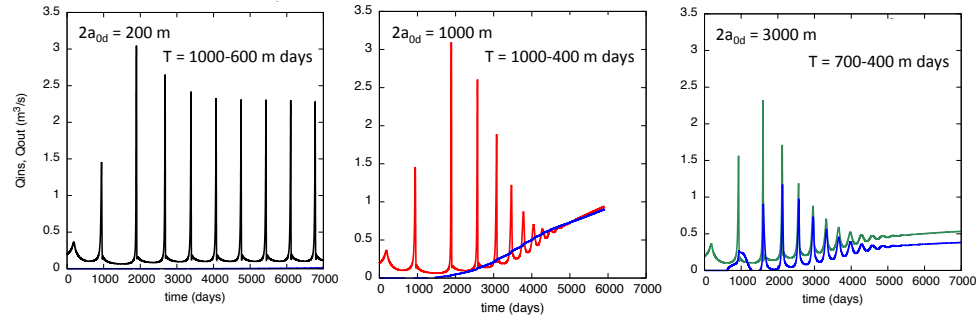


Fixed parameters
 ARs = 1
 ARd = 1
 $V_{chd} = 650 \text{ km}^3$

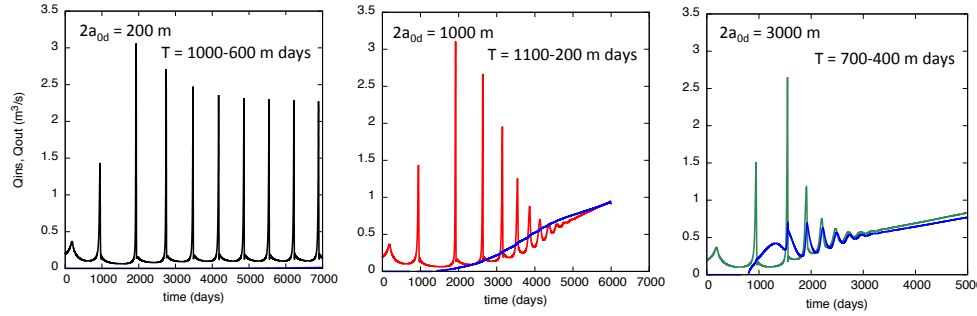
Shallow Chamber Volume
 $V_{chs} = 30 \text{ km}^3$



Shallow Chamber Volume
 $V_{chs} = 40 \text{ km}^3$

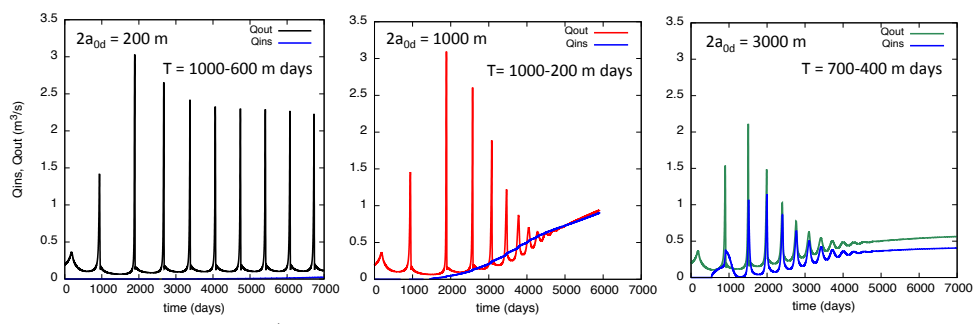


Shallow Chamber Volume
 $V_{chs} = 50 \text{ km}^3$

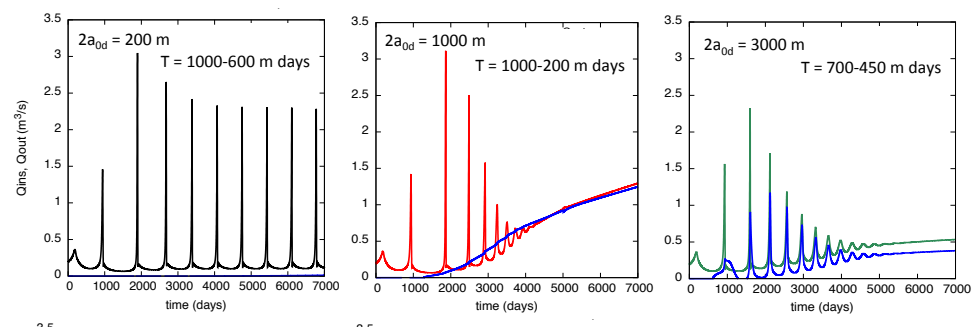


Fixed parameters
 ARs = 1
 ARd = 1
 V_{chs} = 40 km³

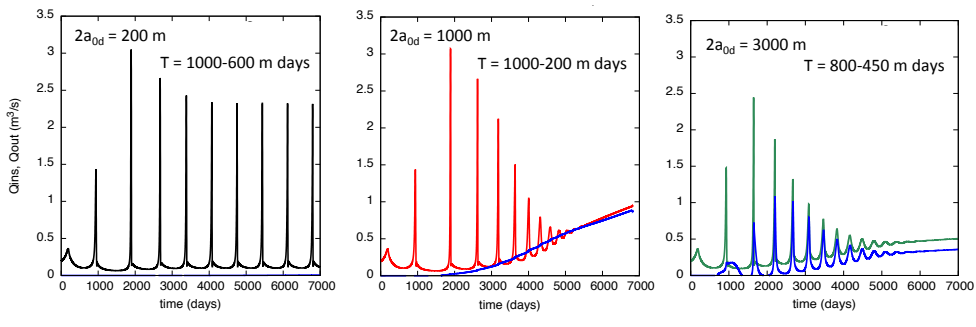
Deeper Chamber Volume
 V_{chd} = 550 km³



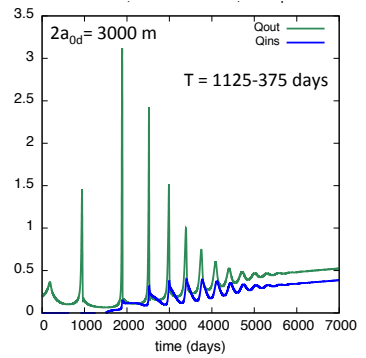
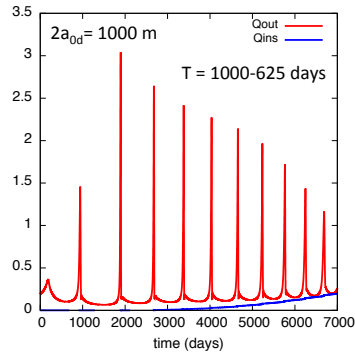
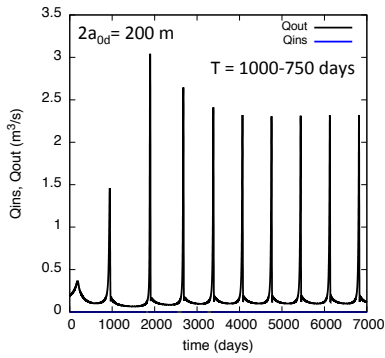
Deeper Chamber Volume
 V_{chd} = 650 km³



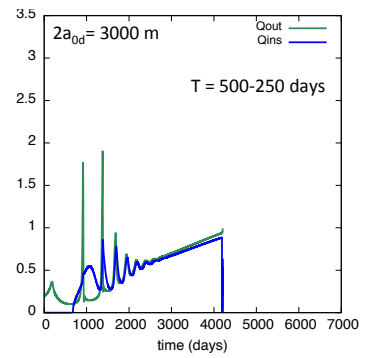
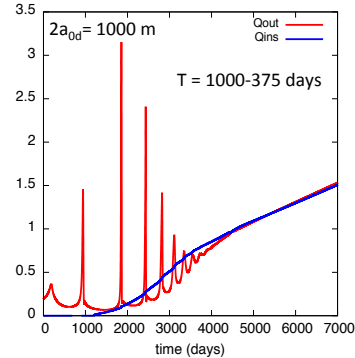
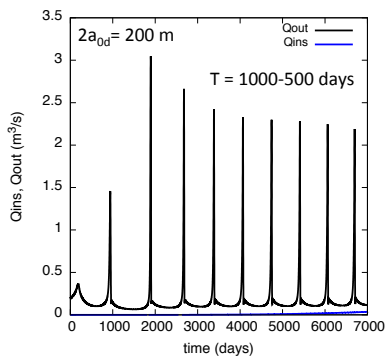
Deeper Chamber Volume
 V_{chd} = 750 km³



▪ $Q_{in_depth} = 1 \text{ m}^3/s$



▪ $Q_{in_depth} = 3 \text{ m}^3/s$



L129

L130

L131

L132

L133

L134

L135

L136

L137

L138

L139

